Simulating pyrolysis of lignocellulosic biomass for bio-oil production and upgrading techniques for sustainable biofuel generation

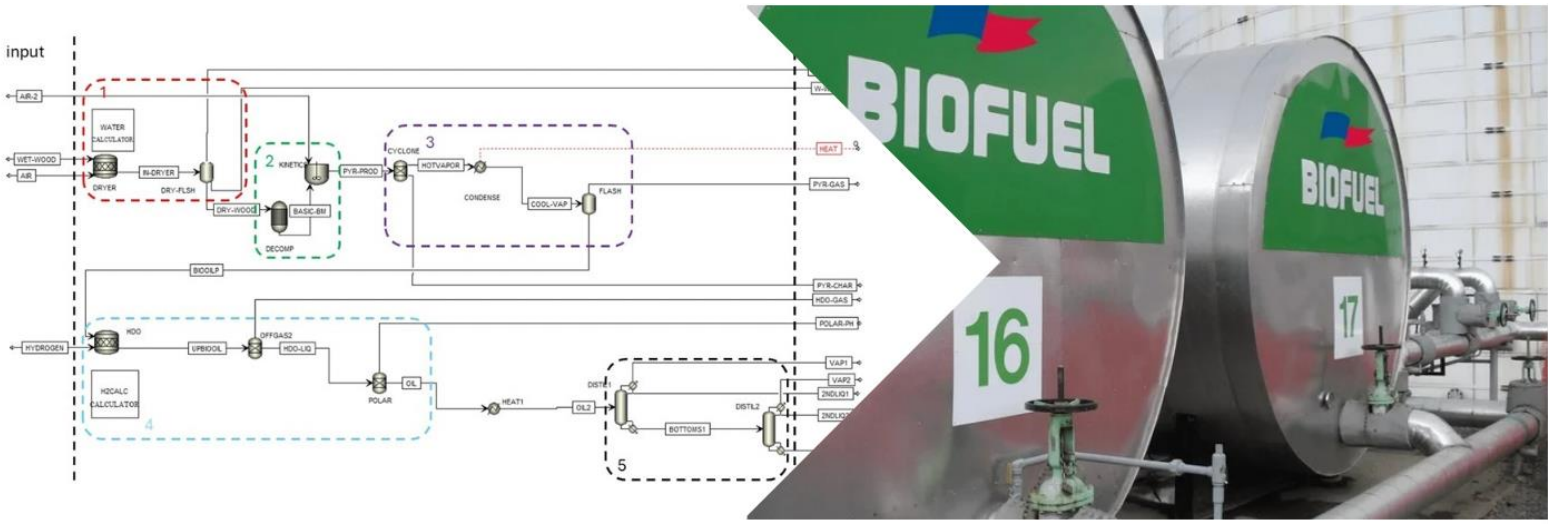

Aspen Plus simulations, comparison of soft- and hardwood bio-oil

Casper de Bruijn

Student number: 4127064
Thesis committee: Prof. Dr. P. Osseweijer
Dr. J. A. Posada Duque
Dr. L. Jourdin

Date: 20-01-2025
Thesis defense: 25-03-2025

TU Delft

Abstract

The ongoing reliance on fossil fuels for transportation poses critical challenges, particularly as global greenhouse gas emissions near irreversible thresholds. While electrification and hydrogen-based technologies offer solutions for some transport sectors, they remain impractical for aviation and maritime applications. Drop-in biofuels, derived from lignocellulosic biomass via thermochemical processes such as pyrolysis, present a viable alternative. Pyrolysis, particularly fast pyrolysis, can efficiently convert biomass into bio-oil, which can then be upgraded to biofuels through hydrotreatment. However, significant challenges remain, including scalability, process optimization, and feedstock variability.

This thesis presents a conceptual process model in Aspen Plus to simulate the thermal decomposition of lignocellulosic biomass into bio-oil and its subsequent upgrading into usable biofuels. The model combines pyrolysis kinetics with hydrodeoxygenation reactions to predict bio-oil and biofuel yields for various feedstocks. Simplifications, including species lumping, were necessary to ensure model feasibility but limited its accuracy and broader applicability.

The results show that the model performs best at pyrolysis reactor temperatures of 550–650 °C and vapor residence times of 2–3 seconds. Hydrodeoxygenation predictions align with literature in terms of hydrogen requirements and overall fuel yield, though limitations in distillation modelling result in a lack of detailed analysis for the fuel fractions. A comparative analysis of softwood and hardwood feedstocks reveals that woods with higher cellulose content yield greater bio-oil and biofuel quantities. However, this comparison overlooks the influence of other factors, such as specific lignin composition and structural differences, which also affect pyrolysis behaviour in real-life applications.

While the model provides insights into pyrolysis and upgrading processes, it demonstrates the need for further refinement to account for complex reaction mechanisms and real-world variability.

Acknowledgements

I can say with great certainty, that completing this thesis has been one of the hardest things I have done in my life. The ups and downs, mental challenges and overall stress has pushed me to places I did not know before, nor wish to go to again. Throughout this long journey (and long it has been…) many people have stood by me who I wish to thank, for without you I would not have been capable to complete it.

I would like to start by thanking John Posada for giving me the project and opportunity to explore it on my own. In retrospect this was not the best decision, but for the lessons I learned about myself I will forever be grateful. The Biotechnology and Society group for their warm welcome, especially the welcome by Elisa, Britta and Haneef in the office we shared.

In particular I would like to thank Sivaramakrishnan Chandrasekaran. After Siva joined the supervisory team in the form of daily supervision my progress increased exponentially. I also enjoyed our in-office discussions, in particular on the subject of Formula 1.

Furthermore, I would like to thank my friends, family and colleagues for their endless encouragements, support and friendly banter. You kept me going when things did not look too great.

The Applied sciences graduation group, all the colleague students and study advisors, for their support. You are what in the end boosted me over the finish line.

And finally, Isabelle, for your patience, your support, your faith in me and above all your love. Thank you.

Contents

List of figures

List of tables

1. Introduction

Fossil fuels currently serve as the primary energy source for transportation and are expected to maintain this role in the foreseeable future (European environment agency, 2024). However, this reliance poses significant challenges, particularly concerning global warming, as greenhouse gas emissions approach irreversible thresholds (World meteorological organization, 2023). The persistent dependence on fossil fuels, compounded by economic priorities, often conflicts with sustainability goals(Holum & Jakobsen, 2024) and no single solution is suitable to address this problem.

In pursuit of alternatives to fossil fuels, various techniques and innovations have been explored, among which biofuels represent a promising option. While electrification and hydrogen-based solutions offer viable pathways for road transport, these alternatives are less practical for sectors such as aviation (Suarez et al., 2024) and maritime transport.

A potential solution lies in the use of drop-in biofuels, which can integrate into existing infrastructure. Biofuels are produced either through biochemical processes, such as bioethanol production, or thermochemical routes. The latter approach offers greater flexibility in terms of feedstock, as it does not compete with food crops and provides additional benefits, including a closed carbon cycle and the valorisation of waste products (Kargbo et al., 2021).

Despite their advantages, biofuels face several challenges. These include scalability, upstream issues such as feedstock collection, storage, handling and pre-treatment, as well as midstream obstacles such as immature technologies and high production costs. Additionally, quality-related concerns such as corrosion, viscosity and stability further complicate their development and application (Bridgwater, 2013).

Among the more mature technologies for bio-oil production is pyrolysis, a thermochemical process in which biomass is decomposed into gas, bio-oil and char through the application of heat in an oxygen-free environment. Fast pyrolysis, in particular, holds promise due to its higher bio-oil yield. This process involves the decomposition of biomass in a fluidized bed reactor at temperatures ranging from 450 to 650 °C, with a vapor residence time of approximately two seconds (Bridgwater, 2013).

However, bio-oil is not directly suitable as a transportation fuel and requires upgrading through hydrotreatment. This process involves cracking large aromatic compounds and naphtha-like molecules while removing oxygen to improve fuel properties (Patel & Kumar, 2016).

To identify optimal process conditions and pathways, computational methods such as process simulations and techno-economic evaluations are employed. Rate-based reaction modelling can be utilized to simulate biomass pyrolysis, while software such as Aspen Plus can be used to analyse the thermodynamics and refine the production process (Peters et al., 2017a).

1.1. Scope of this work and research questions

The pyrolysis process has been extensively studied using process simulations. However, this task presents significant challenges due to the need for major simplifications, as the bio-oil produced during pyrolysis comprises hundreds of compounds. Many studies investigating the pyrolysis process focus on specific feedstocks, relying heavily on experimental data. While effective, this approach is limited in its applicability to feedstocks for which no experimental data exists.

Kinetic models, such as those proposed by (Peters et al., 2017b), address this limitation by enabling the investigation of a broader range of feedstocks. By integrating rate-based reaction models for pyrolysis with subsequent upgrading steps, such as hydrodeoxygenation, these approaches provide valuable insights into the biofuels produced from various feedstocks. Such insights have the potential to facilitate the hypothetical scale-up of pyrolysis processes or identify promising feedstocks for biofuel production.

Previous studies, such as (Ding et al., 2017), have investigated the pyrolysis behaviour of hardwoods and softwoods. However, a direct comparison using a rate-based kinetic model combined with the upgrading of bio-oil to biofuels has not yet been conducted.

This thesis proposes a conceptual process model developed using Aspen Plus for the thermal decomposition of lignocellulosic biomass into bio-oil through pyrolysis, followed by the upgrading of the bio-oil into usable biofuels. This model aims to address the following research questions:

1 Using computational process simulations, what are the key parameters in the thermal conversion of woody biomass during pyrolysis and the subsequent upgrading of the formed bio-oil to biofuel?

2 Can the same model be used to compare and predict pyrolysis outcomes and biofuel products between soft- and hardwood?

2. Materials and method

2.1. Process description

To investigate the key parameters and a comparison between soft- and hardwood a conceptual process design was done concluding the literary review. Based on the results found in the early-stage analysis a concept process is suggested that can investigate both subjects. The process flow diagram can be found in Figure 1 and separates the process in five key sections.

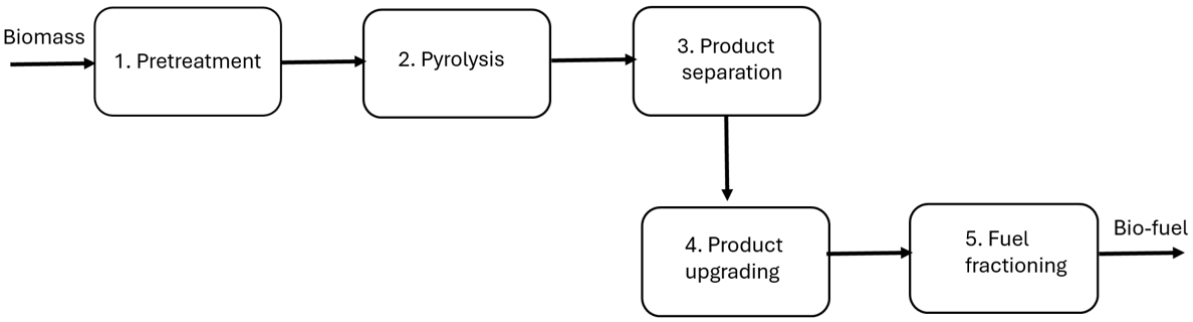

Figure 1 process flow diagram for biofuel production from bio-mass through pyrolysis

Each of these five sections is responsible for a different part of the process. Section 1 is pretreatment, where the wet biomass is dried to the desired moisture content for pyrolysis <10%. Section 2 fast pyrolysis, where the biomass is thermochemically converted to non-compressible gas (NCG), pyrolysis vapours and char. Section 3 product separation, is where the solids are separated from the pyrolysis vapours and NCG, after which the pyrolysis vapours are condensed and separated as bio-oil from the NCG. Section 4 product upgrading, lowers the oxygen content of the bio-oil through hydrodeoxygenation and separates the polar fraction to produce a higher quality fuel. Section 5 fractionates the remaining fuel into three different fuels through distillation.

Following the flow diagram from Figure 1 a process model was built in the process simulating software Aspen Plus v8.8. The evaluation of the model is first done through literary validation and evaluation of biomass is based on product efficiency in fuel/kg feedstock.

2.2. Aspen Plus simulation

This chapter goes over the design choices made for each section, as well as the selected property package and user defined compounds.

2.2.1. Section 1: pretreatment

Pretreatment of the biomass influences the pyrolysis products, it can increase bio-oil yields, higher yields of certain compounds or overall process efficiency. Pretreatments are subdivided into several categories (Amenaghawon et al., 2021): physical, chemical, and biological pretreatment.

For this model, the choice was made to only do thermal pretreatment to decrease the moisture content to <10%. Pyrolysis liquids contain some water, both from the original biomass as from the water created in the pyrolysis reactions. Lower moisture content promotes biochar formation, while a higher moisture content promotes bio-oil formation at higher energy requirements (Huang et al., 2011). It is however important to not go to high in water content as phase separation can occur hence the maximum of <10% moisture content (Bridgwater, 2012).

Aspen Plus block (DRYER): RStoic reactor in conjunction with a water calculator block. The DRYER block first does a fractional conversion of wood to water, which is later specified in the WATER CALCULATOR block to how much wood is converted. This is done because the moisture content of a solid cannot be removed otherwise in Aspen. The moisture content is a part of the proximate analysis and using the WATER CALCULATOR block allows for a fraction of the feed mass to be changed to water which can then be removed in the DRY-FLSH block.

2.2.2. Section 2: fast pyrolysis

Fast pyrolysis in a fluidized bed is simulated by the blocks DECOMP and KINETICS together. DECOMP is a yield reactor where the biomass is first broken up into its biochemical reference compounds: cellulose, hemicellulose and lignin based on the ratios for the biomass as stated in literature. This is for aspen to turn the nonconventional solid compound wood into conventional compounds which can be used to do kinetic reactions. These kinetic reactions take place in the KINETICS reactor, which is a continuous stirred tank reactor, operating at typical fast pyrolysis parameters. From 300 – 600 ℃ and a residence time of 0,1 – 3 s, depending on what is analysed.

The pyrolysis model can be seen as a connected kinetic model of individual decomposition reactions of cellulose, hemicellulose and lignin (Di Blasi, 2008).

Kinetic reactions are used to improve accuracy when describing and predicting the devolatilization of the biomass by giving a rate of weight loss of the reference components and the expected composition of products released into the solid, vapor and gas phases. These stochiometric reactions are described in Table 1 with their rate and activation energy.

Table 1 stoichiometry of devolatilization reactions with their rate and activation energy.

#	STOCHIOMETRY	RATE (/S)	ACTIVATION ENERGY (KCAL/KMOL)	TEMPERATURE EXPONENT N
1	CELL(CISOLID) --> CELLA	8,00E+13	46000	0
2	CELLA(CISOLID) --> 0,95 GLYCO-01 + 0,25 GLYOX-01 + 0,2 ACETA-01 + 0,2 ACETO-01 + 0,25 5-HYD-01 + 0,2 CARBO-01 + 0,15 CARBO-02 + 0,1 METHA-01 + 0,9 WATER + 0,65 CARBON	1,00E+09	30000	0
3	CELLA(CISOLID) --> LEVOG-01	4	10000	1
4	CELL(CISOLID) --> 5 WATER + 6 CARBON	8,00E+07	32000	0
5	HEMC(CISOLID) --> 0,4 HEMC1 + 0,6 HEMC2	1,00E+10	31000	0
6	HEMC1(CISOLID) --> 2,5 HYDRO-01 + 0,125 WATER + CARBO-02 + CARBO-01 + 0,5 FORMA-01 + 0,25 METHANOL + 0,125 ETHAN-01 + 2 CARBON	3,00E+09	27000	0
7	HEMC1(CISOLID) + WATER --> XYLOSE	3,00E+00	11000	1
8	HEMC2(CISOLID) --> 1,5 HYDRO-01 + 0,125 WATER + CARBO-01 + 1,5 FORMA-01 + 0,25 METHANOL + 0,125 ETHAN-01 + 2 CARBON	1,00E+10	33000	0
9	LIG-C(CISOLID) --> 0,35 LIG-CC + 0,1 P-COUMAR + 0,08 PHENO-01 + 1,49 HYDRO-01 + WATER + 1,32 FORMA-01 + 7,05 CARBON	4,00E+15	48500	0
10	LIG-H(CISOLID) --> LIG-OH + ACETO-01	2,00E+13	37500	0
11	LIG-O(CISOLID) --> LIG-OH + CARBO-01	1,00E+09	25500	0
12	LIG-CC(CISOLID) --> 0,3 P-COUMAR + 0,2 PHENO-01 + 0,35 ACRYL-01 + 1,2 HYDRO-01 + 0,7 WATER + 0,25 METHA-01 + 0,25 ETHENE + 1,3 FORMA-01 + 0,5 CARBO-02 + 7,5 CARBON	5,00E+06	31500	0
13	LIG-OH(CISOLID) --> LIG + 0,5 HYDRO-01 + WATER + METHANOL + 0,5 CARBO-02 + 1,5 FORMA-01 + 5 CARBON	1,00E+13	49500	0
14	LIG(CISOLID) --> SINAPYL	8,00E+01	12000	1
15	LIG(CISOLID) --> 0,7 HYDRO-01 + WATER + 0,7 FORMA-01 + 1,3 CARBO-02 + 0,4 METHANOL + 0,2 ACETA-01 + 0,2 PROPI-01 + 0,4 METHA-01 + 0,5 ETHENE + 6,2 CARBON	1,20E+09	30000	0

These reactions are kinetically expressed by power law reactions in Aspen Plus as described in equation 1 below.

$$1. \quad r = k * T^n * e^{\frac{-E}{RT}}$$

Where r is the rate of reaction, k the pre-exponential factor, T temperature in degrees Kelvin, n temperature exponent, E activation energy and R gas constant.

For the reactor the choice was made to simulate the fluidized bed reactor by a CSTR block. A continuous stirred tank reactor in Aspen Plus can simultaneously do equilibrium reactions and rate-based reactions accurately when reaction kinetics are known (Aspen Technology, 2001).

2.2.3. Section 3: pyrolysis product separation

Hot pyrolysis product separation starts in the CYCLONE block. Here 100% of all solids remaining are removed and classified as pyrolysis char. The remaining product is then cooled and using the FLASH block liquid and gas are separated. The FLASH operates at 20 ℃ and 20 bar, with vapour-liquid-liquid as valid phases, this is because bio-oil can be considered a micro-emulsion of several liquid phases (oil and aqueous), both stable and un-stable (Bridgwater, 2012). The gas is then a final product and classified as PYR-GAS. The liquid is classified as BIOOILP and continues to be hydrotreated.

2.2.4. Section 4: hydrodeoxygenation

To make a quality bio-oil fuel the pyrolysis oil product needs to be upgraded, this can be done in several ways, physically, chemically and catalytically. For this model, the focus lies on transport fuel production where full deoxygenation is required as well as conventional fuel refining (Bridgwater, 2012). Hydrotreatment of bio-oil is done by removing oxygen from the oil as water through a catalytic reaction with hydrogen. It is generally done under high pressure 50 to 200 bar and temperatures of 200 and 400 ℃ (Han et al., 2019a).

Table 2 Hydrodeoxygenation of 5-Hydroxymethylfurfural.

FORMULA	COMPOUND	KG/H	C	H	O
C6H6O3 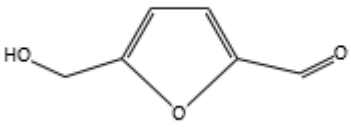	5-HYD-01	119,488	6	6	3
	$C_6H_6O_3 + 3H_2 \rightarrow C_6H_8O + 2H_2O$ (Brandi et al., 2020)				

As the bio-oil comes into the hydrodeoxygenation unit (HDO) it is processes at 400 ℃ and at 1 bar (the pressure did not affect the process). The required oxygen is calculated using the H2CALC block, this block calculates the hydrogen separately for each of the bio-oil products to be deoxygenated. The reactions for each bio-oil product are added manually an example of such a reaction is shown in Table 2, the rest of the reactions can be found in appendix 6.1. HDO reactions.

2.2.5. Section 5: fuel fractioning

After hydrotreatment the final bio-oil product is distilled to fractions into three fuels based on the components boiling points (Olarte et al., 2017). The oil is first heated to 200 ℃ at 3 bar and then enters the first distillation column DISTIL1. The first column operates at 2,9 bar over seven stages and the oil entering at stage four (full parameters can be found in appendix 6.2. Model summary). This results in three streams VAP1 (small components and remaining water), 2NDLIQ1 (gasoline range products) and BOTTOMS1 (lower boiling point products). BOTTOMS1 is then further distilled in DISTIL2 over 3 stages. This results in two more fuel products 2NDLIQ2 (jet fuel range) and OIL3 (diesel and rest fuel range).

2.2.6. Property package

The property package used to estimate the physical properties of the conventional components is Peng-Robinson equation of state with Boston-Mathias alpha function (PR-BM). With this property package standard mixing rules apply, which are recommended for hydrocarbon processing applications such as gas processing, refinery and petrochemical processes (Aspen technology inc., 2013).

The alpha parameter in this property package is a temperature dependent variable that improves vapor pressure simulations at high temperatures such as in gasification and can be applied to pyrolysis (Ramzan et al., 2011). In (Aspen technology inc., 2013) it is also stated that PR-BM is suited for hydrocarbon applications at higher pressures processes such as HDO.

2.2.7. Component database and user defined compounds

Most components and their physical properties are in the Aspen Plus databases and any missing properties are estimated using the Aspen engine. However as Aspen Plus is mostly used in petrochemical applications it does not have many biochemical components readily available in its databases. For the components that are not available their properties are found through literary research.

The property package PR-BM requires at a minimum the molecular weight, solid heat of formation, solid molar heat capacity and solid molar volume for solid compounds. These are described by (Wooley & Putsche, n.d.-a), (Peters et al., 2017b) and (Gorensek et al., 2019), this together with the chemical structure is then used by Aspen Plus to estimate the missing parameters and functional groups. An example for hemicellulose can be found below in Table 3, the rest of the user defined components can be found in the appendix 6.3. User defined components.

Conventional components require at a minimum values for: molecular weight, ideal gas standard heat of formation, critical temperature, critical pressure, acentric factor, vapor pressure and ideal gas molar heat capacity parameters. These were found for the components p-coumaryl alcohol and sinapyl aldehyde and can be found in appendix 6.3. User defined components.

Table 3 example of user defined component hemicellulose, which is represented in the model by Xylan, data taken from (Wooley & Putsche, n.d.-a) *and (Gorensek et al., 2019).*

COMPONENT	**CHEMICAL STRUCTURE**	
Hemicellulose	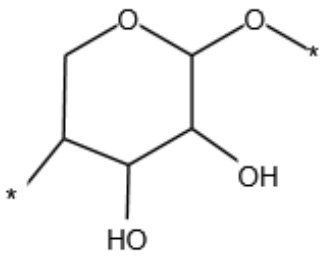	MOLECULAR WEIGHT G/MOL: 132,11 SOLID ENTHALPY OF FORMATION (KJ/KMOL) -759200 SOLID MOLAR HEAT CAPACITY (KJ/KMOL-K): 162,72 SOLID MOLAR VOLUME (ML/MOL): 86,92

2.3. Process validation and evaluation

2.3.1. Pyrolysis

To Validate the model as a predictive tool, it is checked against literary data. In general, yield curves with different temperatures or residence times can be used, to see if they describe a similar pyrolysis weight loss profile as the model. For a more in-depth validation a full set of biomass property parameters are needed (biochemical composition and elemental composition), in addition to the weight loss data. This is because even biomass from the same species can vary significantly in composition and thus reduce the accuracy of the validation (Peters et al., 2017b).

Full composition is given for the following hardwood's: eucalyptus by (Oasmaa et al., 2010) and beech (Peters et al., 2017b) and for softwood's: Chinese fir by (Ding et al., 2017) and pine by (Oasmaa et al., 2010).

Validation and evaluation is done by comparing weight loss curves and final yield for bio-oil, char and gas at specific temperatures and residence times. This can be done for complete streams/feedstock as well as individual compounds.

2.3.2. Fuel production

Comparison of fuel production is done based on yield of total fuel from the bio-oil and fraction yields for the different fuel types. Hydrogen consumption is compared to typical hydrogen consumption for bio-oil upgrading.

2.3.3. Wood comparison

Hard- and soft-wood will be compared on their product efficiency (kg bio-oil/kg feedstock) and the hydrogen consumption to upgrade the bio-oil to fuel (kg hydrogen/ kg bio-oil). The biochemical composition for these woods can be found in appendix 6.4. Biochemical composition for different wood types.

2.3.4. Sensitivity analysis

The nature of pyrolysis modelling requires simplification due to the complexity of the process; each simplification brings with it a measure of uncertainty and or inaccuracy in the output of the model. To get a feeling for which input parameters play a significant role and which do not a sensitivity analysis was done. This is done by changing the input parameters by small steps and measuring the effect on the modelling output. There are three classes of sensitivity analysis; screening, local and global (Nyazika et al., 2019). In this case only a screening was done, which provides qualitative insight for the input parameters. The investigated input parameters for the model are as follows:

- Pyrolysis reactor temperature (˚C)
- Vapour residence time in reactor (s)
- Biochemical composition (wt)
- Kinetic parameters

For this sensitivity analysis only the reactor temperature and vapour residence time are evaluated.

3. Results and discussion

3.1. Fast pyrolysis combined with hydrotreatment model

This thesis presents a kinetic model that can calculate yields and to an extend give the composition of fast-pyrolysis products using lignocellulosic biomass as a feedstock. The resulting pyrolysis bio-oil is then further processed to biofuel and separated into gasoline, jet-fuel and diesel. Using Aspen Plus to run the model allows for process analysis independent from experiments and give insight into the influence of reactor conditions and feedstock composition. Thus, the model allows for quick analysis of pyrolysis product yields and subsequent fuel products using minimal input.

An overview of the complete model as implemented can be found in Figure 2, with complete block settings found in appendix 6.2. Model summary. Input settings required for the model are described in Table 4, these can often be found in literature, databases like phillis or by experiments.

Table 4 Biomass input parameters for the model.

PROXIMATE ANALYSIS WEIGHT%	**BIOCHEMICAL COMPOSITION WEIGHT%**
Fixed carbon	Cellulose
Volatile matter	Hemicellulose
Ash	Lignin
Water	

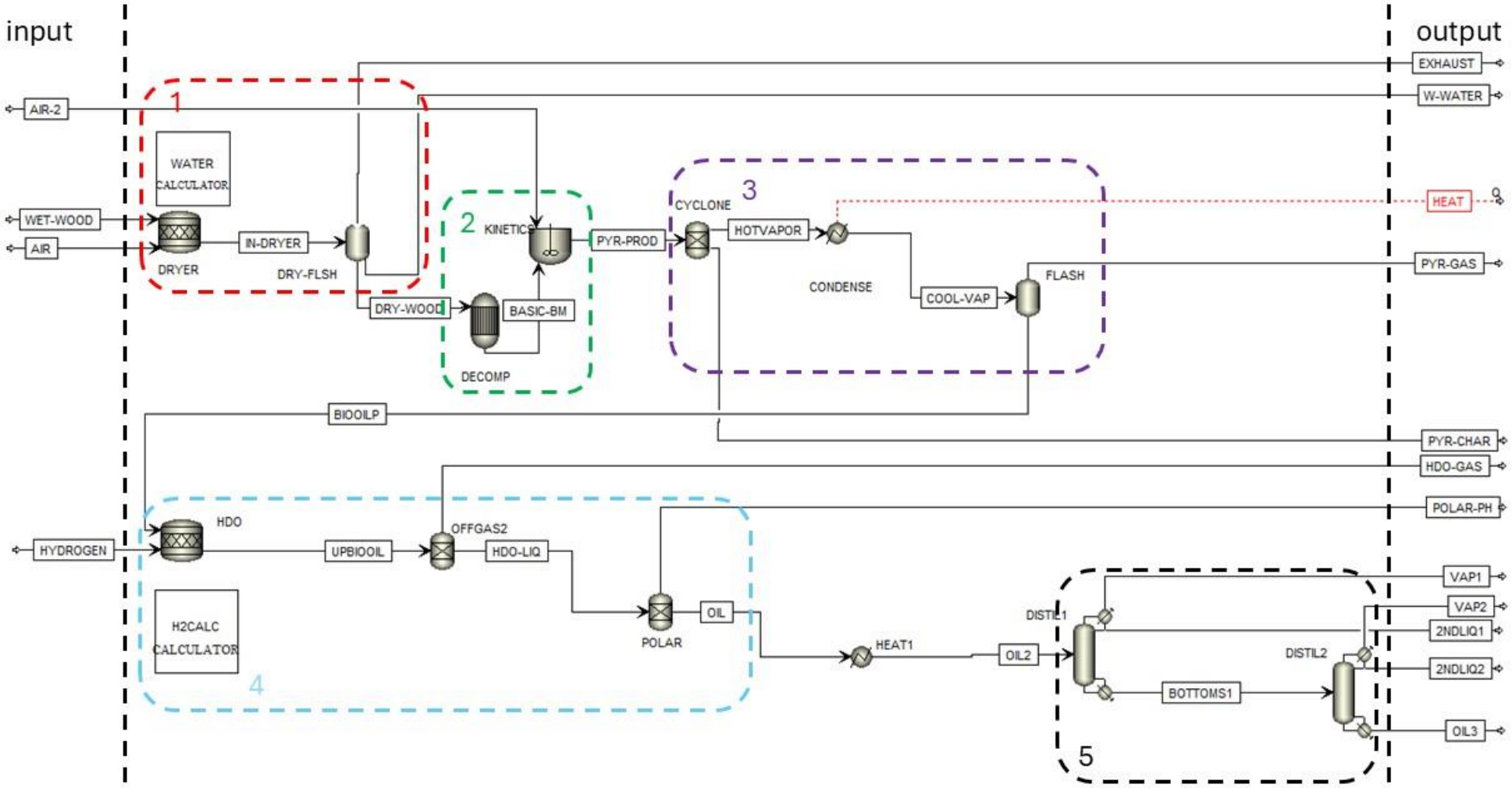

Figure 2 Biofuel production model as presented in Aspen Plus. With to the left incoming streams and to the right outgoing streams. Labelled sections: 1: preprocessing, 2 pyrolysis, 3 pyrolysis product seperation, 4 Hydro-deoxygination and 5 fuel fractioning.

3.2. validation and comparison

3.2.1. pyrolysis validation

The validation is done in three steps, first compare biomass weight loss to known thermogravimetric data, next zoom in and compare liquid, gas and solid yields to literature and thirdly look at weight loss of individual biochemical compounds and compare to literature.

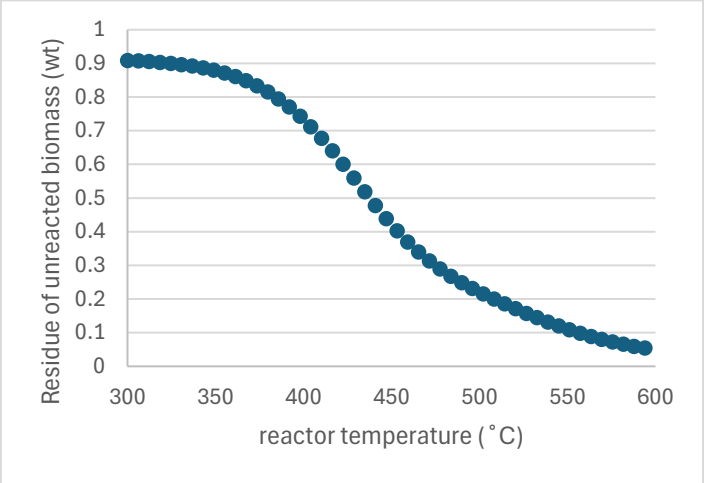

Figure 3 solid biomass weight loss as a function of the reactor temperature (ºC) from the model.

Figure 3 shows a typical weight loss profile of lignocellulosic biomass undergoing thermal decomposition through fast pyrolysis. Comparing Figure 3 to (Mishra et al., 2015) the decomposition rate is not as fast, but at higher temperatures does agree (above 550℃) in remaining biomass.

Zooming in to validate sections 1, 2 and 3 a comparison is made between output streams from the pyrolysis reactor of liquid, solid and gas and experimental results. Specifically, experimental work using lignocellulosic feedstock and a fluidized bed pyrolysis reactor, such as the work of (X. Wang et al., 2005) as seen in Figure 4. As well as specific comparison between individual pyrolysis mass loss of Cellulose, Hemicellulose and lignin within a typical fast pyrolysis range for the reactor temperature (°C).

According to (Paperi & Hawboldt, 2015) biomass decomposition takes place in three stages; in the first stage (<200 ºC) water, carbon monoxide and carbon dioxide are released, the second stage (475 to 655 ºC) the main decomposition takes place and in the third stage (600> ºC) the decomposition slows down. Cellulose and Hemicellulose are decomposed in the second stage where lignin is decomposed over the second and third stage, this is also shown in Figure 5.

As seen in Figure 4 the results from the model do not follow the results closely as presented by (X. Wang et al., 2005). The error margin is particularly large outside of the 550-650 ℃ range. Typical fast pyrolysis temperature range is 400-550 ºC where liquid yields are the highest (Kan et al., 2016).

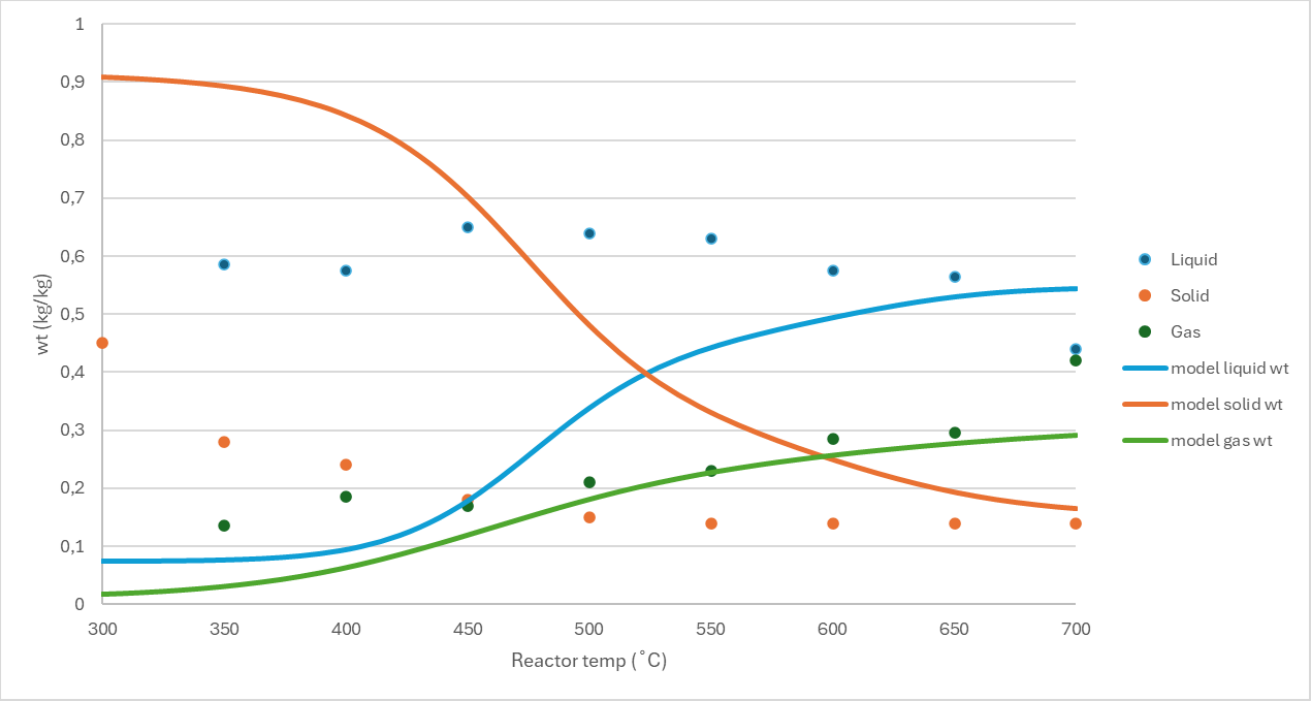

Figure 4 comparison of gas, liquid and solid yields between pyrolysis predictions from the model (lines) and literature (dots) from (X. Wang et al., 2005).

Looking at the first stage in Figure 4 the solid fraction is large below 400 ºC, indicating that very little decomposition has taken place, where in the experimental data a large fraction has already been decomposed. Part of this can be contributed to the simplification of biomass, as it is simplified to water, cellulose, hemicellulose and lignin, of which the last three cannot be released at lower temperatures.

Furthermore, at temperatures between 200 and 400 ℃ a melt phase reaction takes place for the lignin components, in this phase the compounds depolymerize and condensate (Frassoldati et al., n.d.). In the initial model reactions -the products are still classified as solids, as they are unreacted biomass in the final product and thus solid. This also contributes to the overestimation of solid yield at lower temperatures. This melt phase starts at lower temperatures for cellulose and hemicellulose <250 ℃.

At temperatures above 600 ℃ most of the cellulose and hemicellulose has been decomposed as can be seen in Figure 5, the unreacted lignin components however continue to decompose at higher temperatures. This results in an increasing liquid yield at higher temperatures. While this holds true specifically for lignin, it does not take in account the increased carbon formation at higher temperatures (charring) from all other components, which would detract from liquid yield and add to the solid yield.

Another influence on bio-oil yield are the secondary pyrolysis reactions taking place in the vapour phase. These decrease bio-oil yield and increases gas and solid yields, the reactions are more significant at longer pyrolysis times and less so for fast pyrolysis times <2s. Even so they can result in a slight overestimation of liquid phase and underestimation of solid and gas phase. Other influences on these secondary gas phase reactions are the temperature and the alkali metal content in the ash, as the alkali metals catalyse these reaction (Aho et al., 2013). These are however not corrected in the model.

When looking at the individual biochemical compounds it is noted that a high percentage of unreacted Lignin-OH is left after pyrolysis (factor four compared to other lignin compounds), this also contributes to a high solid yield. Lignin-OH is degraded following reaction 13 from Table 1 with a rate of 1e13 s-1 solid enthalpy of formation of -1429200 KJ/Kmol and activation energy of 49500 Kcal/Kmol:

LIG-OH(CISOLID) --> LIG + 0,5 HYDRO-01 + WATER + METHANOL + 0,5 CARBO-02 + 1,5 FORMA-01 + 5 CARBON

Out of all the kinetic reactions it has the highest activation energy requirement all be it at one of the highest rates, which results in a high remainder of Lignin-OH at lower temperatures. Since lignin-OH is formed from Lignin-O and Lignin-H it represents a large part of the lignin fraction and since the three fractions are divided equally a substantial part of the remaining lignin in the char is lignin-OH.

This is also represented in Figure 5 where three stages can be seen first at around 380 next at 420 and last at 600, where the three different lignin types each have different activation energies and each have 1/3 of the weight. This 'discontinuation' in the release of different compounds is also noticeable in experimental data as shown by (Faravelli et al., 2010). It is however more pronounced in the model output due to the simplification of the lignin compounds and reactions.

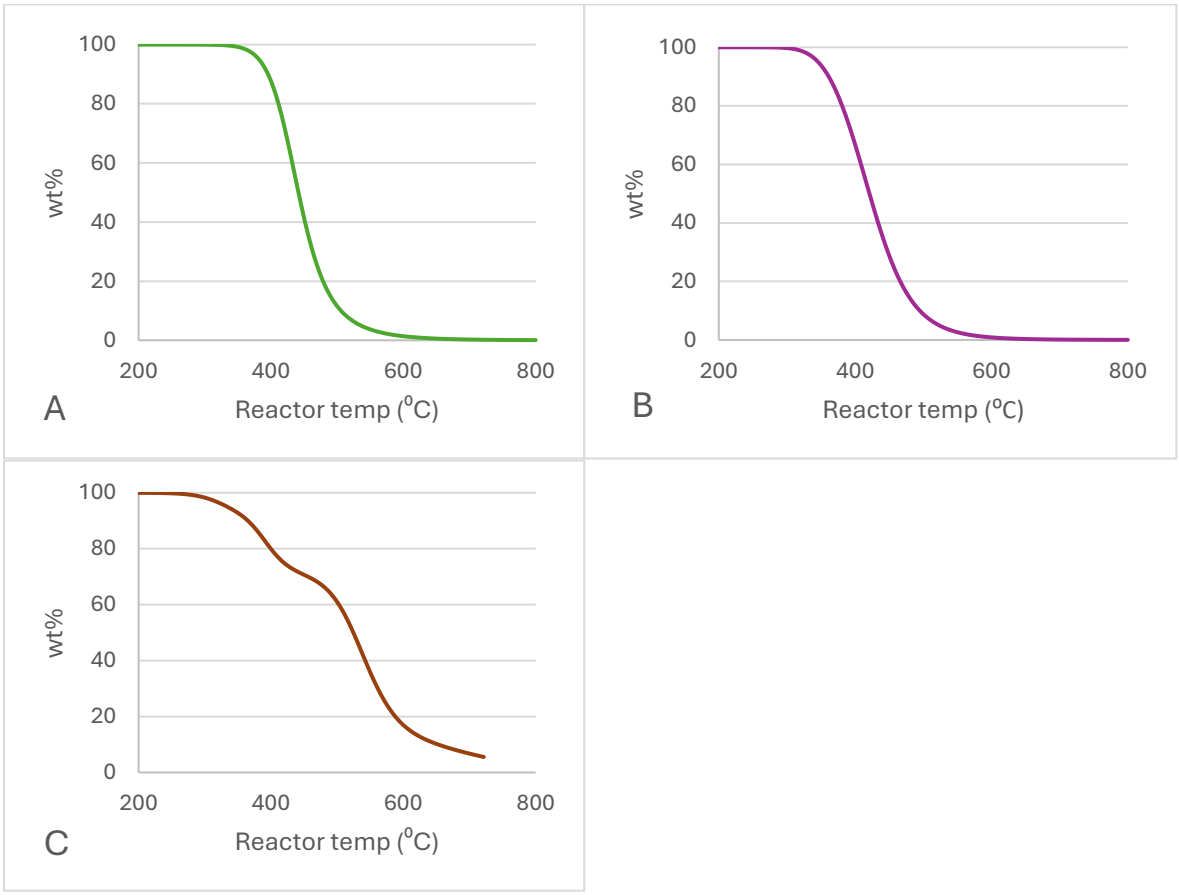

Figure 5 thermal decomposition of cellulose (A), hemicellulose (B) and lignin (C) at varying reactor temperature (°C) and set residence time (s).

Thermal decomposition of hemicellulose and cellulose from Figure 5 agree with the experimental data shown by (Cuoci et al., n.d.). Main difference is seen for hemicellulose as in the model it goes to zero and in the experimental data around 20 wt% is left unreacted. However, this is only the case when hemicellulose is assessed by itself in the model, around 9 wt% of unreacted hemicellulose remains at residence time of 2s and 500 Ċ for pine.

3.2.2. individual biochemical compound contribution to streams

Another interesting way to look at the individual biochemical compounds is to see the contribution to the product streams from the pyrolysis reactor. Figure 6-7 show the contribution per biochemical compound to Bio-oil, char and gas, respectively.

Cellulose shows a high contribution to the bio-oil stream up to 0,82 wt (kg bio-oil/kg dry cellulose) at a 550 Ċ reactor temperature, with a decrease in char (unreacted biomass) and increase in non-condensable gas at higher temperatures. This makes sense when looking at the kinetic reactions in Table 1. The majority of compounds found in reaction 2 and 3 for cellulose contribute to the liquid product like levoglucosan and 5-HMFU, while outnumbering the non-condensable gasses like CO2 and CO as well as the solid carbon (char).

These reactions also have a lower activation energy then reaction 4 which is responsible for the majority of the char formation from cellulose, resulting in an increase in char at higher temperatures (that is not unreacted biomass). This is comparable to the work of (Ansari et al., 2019), which shows a distribution of wt%: 7.04, 84.99 and 8.79 for gases, bio-oil and char, respectively.

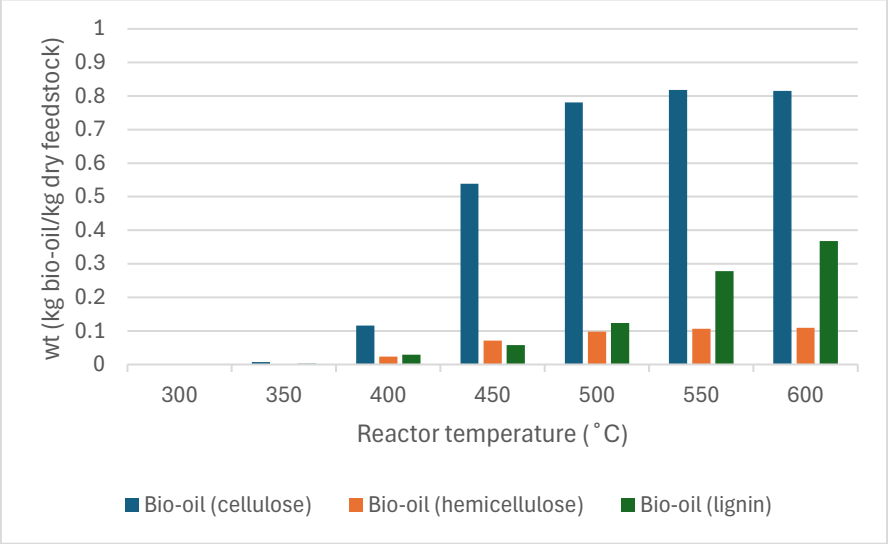

Figure 6 Bio-oil yield for isolated biochemical components at different temperatures (Ċ).

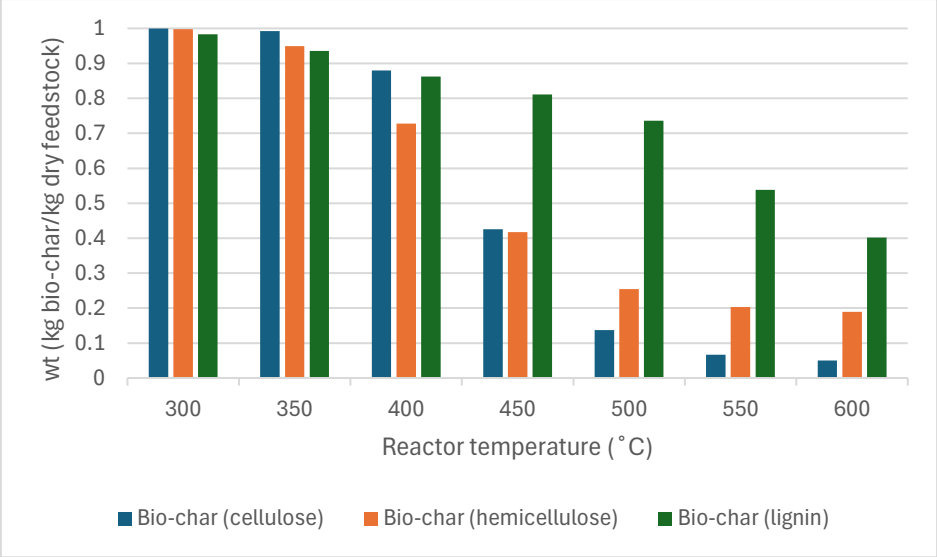

Figure 7Bio-char yield for isolated biochemical components at different temperatures (˚C).

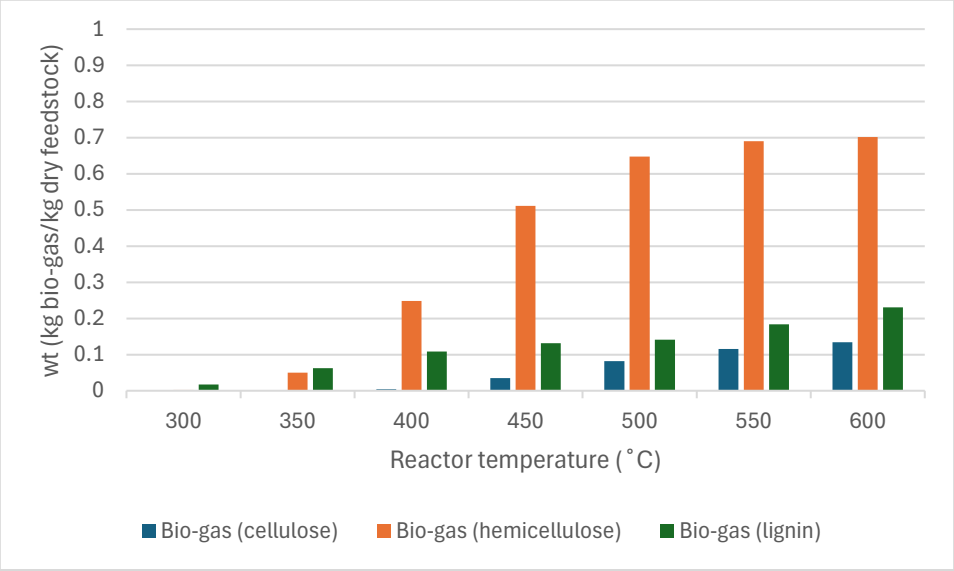

Figure 8 Bio-gas yield for isolated biochemical components at different temperatures (˚C).

For hemicellulose the largest fraction goes to the gas stream, as is expected when looking at the reactions 6 and 8 in Table 1, a large portion of the products are products that end up in the non-condensable gas fraction after pyrolysis. The decrease in the solid fraction at higher temperatures is the decrease in unreacted biomass.

Looking at literature reported yields (Ansari et al., 2019) and (Zhao et al., 2017) hemicellulose is the largest contributor to the gas fraction on a wt/wt basis. The model however overestimates the contribution to the gas fraction and underestimates the bio-oil fraction for hemicellulose, for example at 500 ℃ this is 0.4 wt higher and 0.25 lower, respectively. This would suggest that the product distribution used in the simplification of the kinetic reactions is not accurate.

Lignin bio-oil fraction increases as the temperature goes up; this is due to more unreacted lignin being converted. The reactions in Table 1 show the highest activation energy for lignin compounds, so a decrease in unreacted lignin at higher temperatures makes sense, as well as the increase in bio-oil and gas yields. The char fraction becomes smaller, but the distribution changes towards more carbon than unreacted biomass.

When comparing to (Zhao et al., 2017) and (Ansari et al., 2019) agreeable product distributions are shown at temperatures above 550 ℃, but large underestimations in bio-oil yields below that. This would indicate that the kinetic reactions are not accurate at lower temperatures, this could be adjusted by re-evaluating the activation rate and activation energy of the kinetic reactions, as well as a re-evaluation of the lignin sub-species distribution.

3.2.3. Comparison of bio-oil upgrading and production separation

The one upgrading step done in the model is through hydrotreatment, in this case full oxygen removal by hydrogen reacting with the bio-oil under high pressure and temperature. Table 5 shows around 0,05 wt of kg hydrogen/kg bio-oil, which is comparable to what is referenced by (Shemfe et al., 2015) and typical hydrogen consumption mentioned by (Han et al., 2019b). The latter shows non complete oxygen removal, also lower hydrogen consumption under continuous conditions.

Table 5 comparison of hydrogen consumption during HDO for four different woods and typical HDO from literature.

WOOD	KG HYDROGEN/KG BIO-OIL	NL/KG BIO-OIL	OXYGEN CONTENT %
Eucalyptus	0,05	651,11	0,00
Beech	0,05	634,67	0,00
Pine	0,05	639,14	0,00
Chinese Fir	0,06	659,06	0,00
Source			
(Han et al., 2019b) continuous		600,00	0,3 - 0,6
(Han et al., 2019b)batch		100 - 300	1,0 - 16,0

Table 6 shows very comparable fuel yields in terms of kg fuel/kg of dry feedstock when compared to (Bridgwater, 2013).

Table 6 Comparison of fuel and bio-oil yields from four different wood species typical fuel yields from literature.

	DRY BIOMASS	WET BIOMASS	BIO-OIL
Wood	kg fuel/kg feedstock	kg fuel/kg feedstock	kg fuel/kg bio-oil
Eucalyptus	0,29	0,23	0,53
Beech	0,29	0,23	0,57
Pine	0,25	0,21	0,52
Chinese Fir	0,28	0,23	0,53
Source			
(Han et al., 2019b)continuous			0,30 - 0,68
(Han et al., 2019b)batch			0,17 - 0,92
(Bridgwater, 2013)	0,25		

*Table 7 Literary fuel fractions for hydrotreated pyrolysis oil. *wt% >100 due to overlap between diesel and jet fraction.*

FRACTION	BOILINGPOINT RANGE (˚C)	WT%*	
	(Olarte et al., 2017)	Pine (Wang et al., 2015)	whole pine (Howe et al., 2015)
Gasoline	<184	47,9	42
Jet	184-250	25,1	14
Diesel	150-250	37	44
Residual	>338	15,1	11

Looking at the distribution of different fuel fractions in Figure 9 it is clear that the fractions are very similar for each compound, as well as for pine. The total amount of fuel will differ, but the distribution will not. This shows that the distribution of the fuel fractions is not dependant on the bio-oil composition in the model, just on the way the distillation is set up. This would mean that no relevant conclusion can be drawn from the fuel fractions from different biomass using this model.

Comparing the fractions from *Figure 3*Figure 9 to literature from Table 7, it shows that the diesel fraction is very similar, but the jet and gasoline fractions are quite far off. This is due to a bias for jet range fuel in the distillation column in the model.

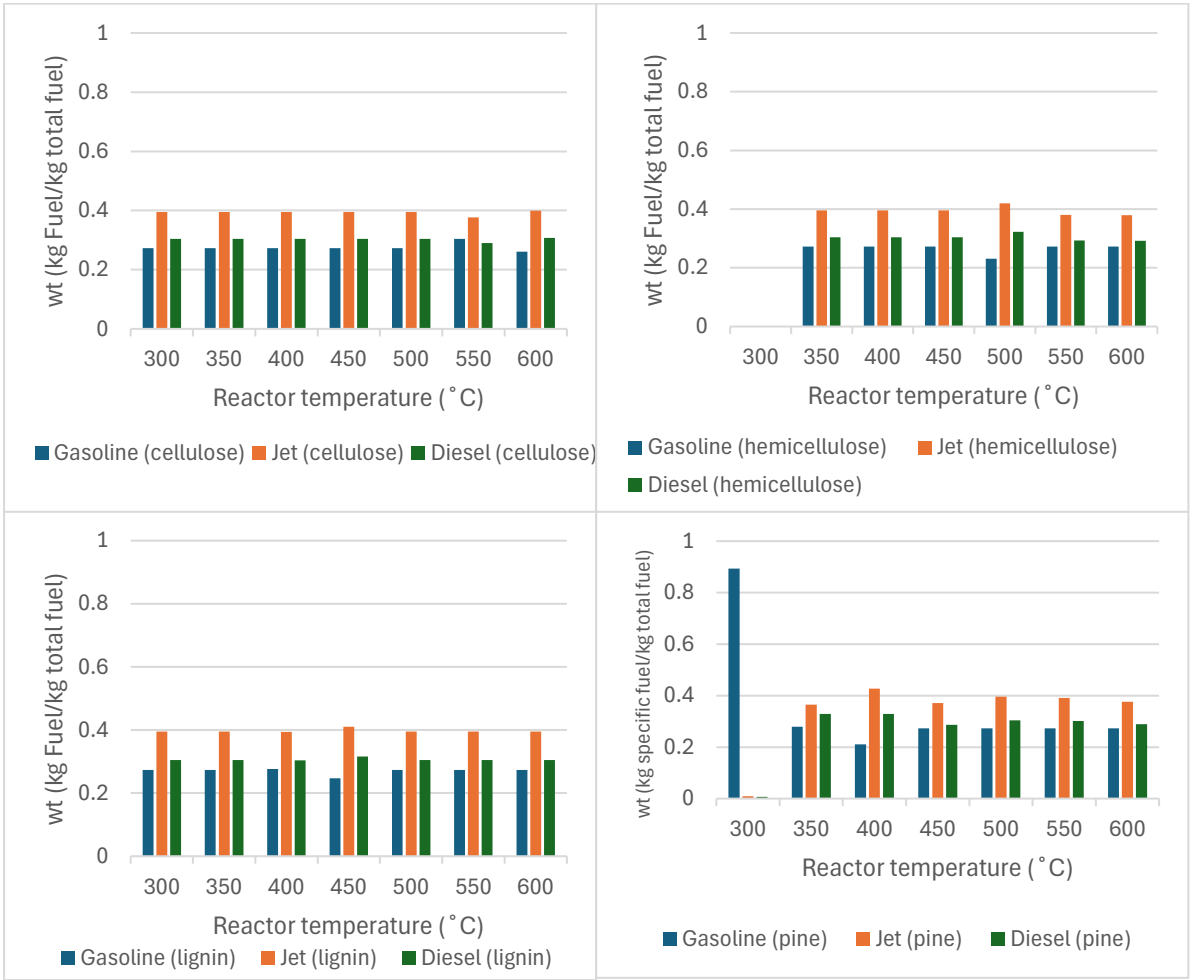

Figure 9 Fuel distribution for individual biochemical compounds (cellulose, hemicellulose and lignin) and pine.

3.3. sensitivity analysis

In order the see the influence of vapour residence time and the reactor temperature two graphs were made as seen in Figure 10. For longer residence times bio-oil yields will keep increasing until all biomass has reacted. The longer the reaction goes on, the more unreacted biomass is degraded, mainly the lignin's, resulting in lower solid yields and higher oil and gas yields. What however is not represented are the secondary reactions that are not present in the model and are more significant at higher residence times. These secondary reactions take place in the vapour phase and break compounds down into smaller components, resulting in more solid carbon and gas production and lower bio-oil yields.

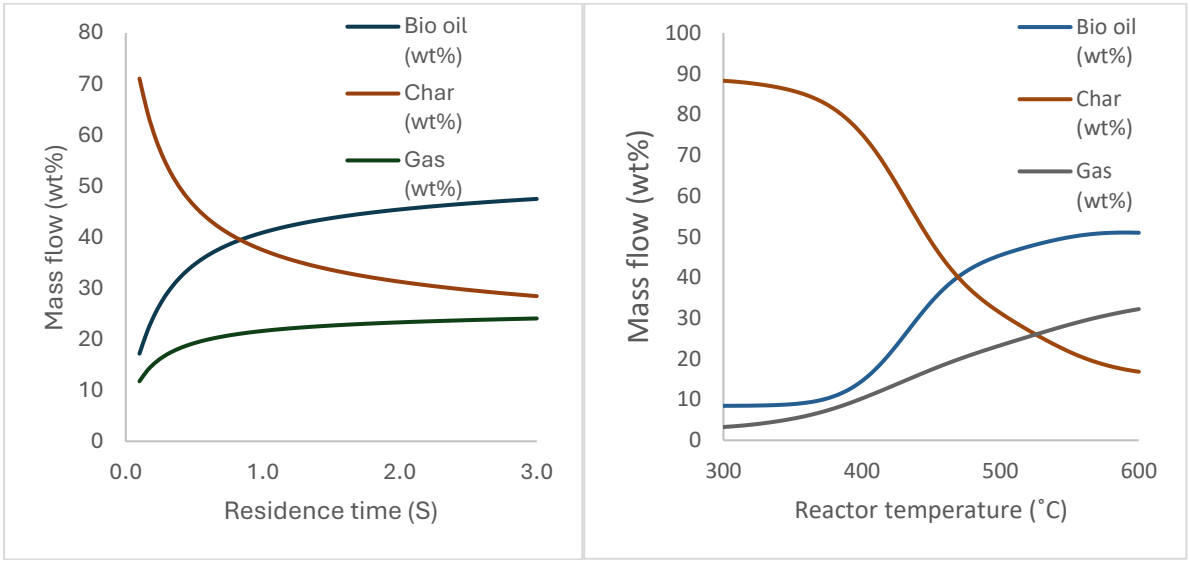

Figure 10 sensitivity analysis of residence time (s) (at 500 ℃) and Reactor temperature (℃) (at residence time of 2s).

Reactor temperatures increase bio-oil yield up to around 590 ˚C, as the temperature increases the kinetic reactions responsible for the char formation start to play bigger roles, due to these reactions having a higher activation energy.

3.4. Comparison between soft- and hardwood

As seen in chapter 3.2.3. Comparison of bio-oil upgrading and production separation no distinctions can be made between fuel fractions of different biomasses, therefore only a comparison is made in terms of bio-oil yield and hydrogen consumption during upgrading.

Figure 11 shows eucalyptus and Chinese fir as having the highest yields under comparable pyrolysis conditions and Beech and Pine trailing. Looking at chapter 3.2.3. Comparison of bio-oil upgrading and production separation this would make sense as eucalyptus and Chinese fir are the species highest in cellulose content, which has the highest yield towards bio-oil.

Proportional difference in the biochemical composition is however not the only difference between hard- and soft-woods. Chemically there are differences between the main macromolecules. In hardwood the hemicellulose backbone is mainly made up of xylose units and in softwood of mannose and glucose units, also in the lignin there are differences in the aromatic rings (Ding et al., 2017).

Also, the sample size of four species, one of each wood type cannot paint a full picture. Using the model the only conclusion that can be drawn is that wood species with higher cellulose content produce higher bio-oil yields.

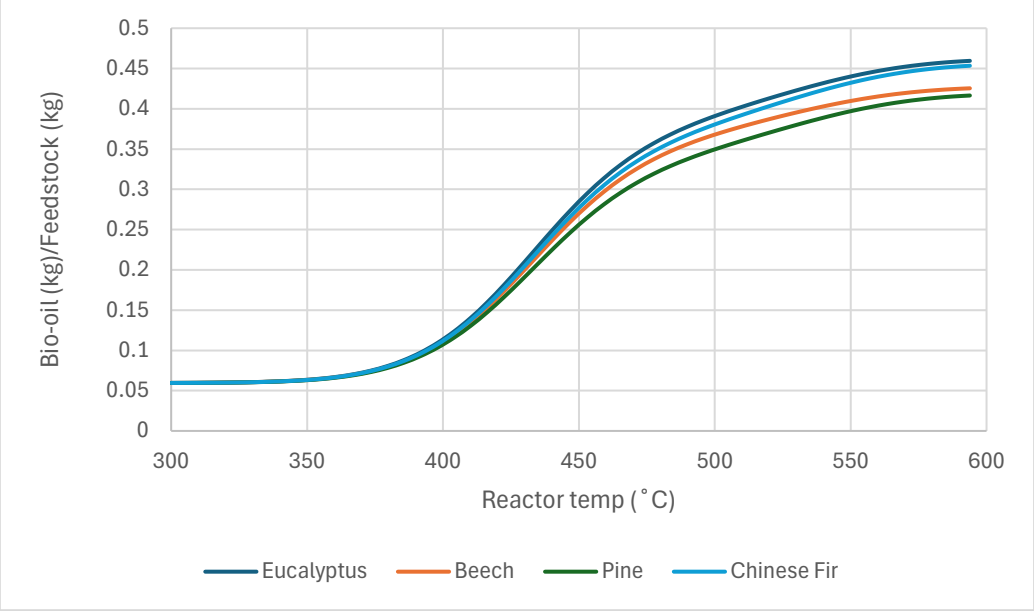

Figure 11 Comparison of hard- and softwoods on their Bio-oil yields (kg/kg feedstock) at different reactor temperatures.

When looking at the hydrogen consumption during HDO in Figure 12 it shows highest hydrogen consumption per kg of bio-oil for eucalyptus and Chinese fir. This once again comes down to a higher cellulose content, which contains more oxygen species that must be removed through HDO.

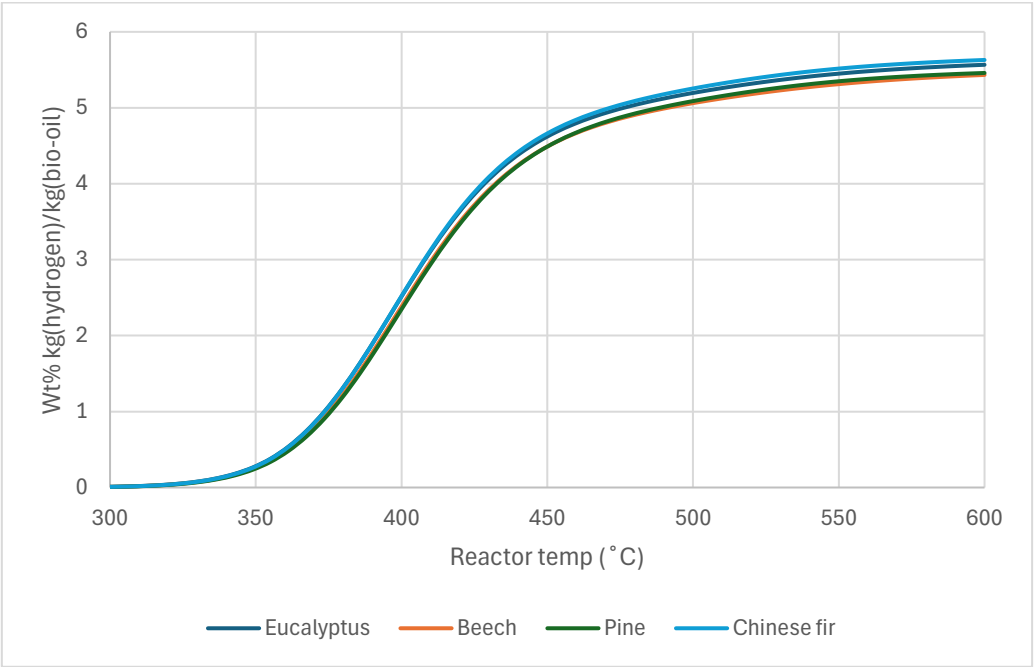

Figure 12 Comparison of hard- and softwoods on their hydrogen consumption during HDO (kg hydrogen/kg bio-oil) at different reactor temperatures.

4. Conclusion and future recommendations

4.1. Conclusion

This thesis presents a model that uses a combination of pyrolysis kinetics and individual hydrodeoxygenation reactions in an Aspen Plus environment to predict bio-oil and biofuel yields for lignocellulosic feedstock.

Due to the complex nature of the pyrolysis reactions and bio-oil product several simplifications and lumping of species were made to keep the goal of a working model attainable. This came however at a cost to accuracy and applicability of the model. The model is most accurate in a range for the pyrolysis reactor temperature of 550 – 650 ℃, which falls just on the edge of typical fast pyrolysis and a vapour residence time between 2 and 3 seconds.

The hydrodeoxygenation shows similar hydrogen requirements to literature as well as the total fuel yield. The fuel fractions however are predetermined through the way the distillation is set up, allowing no real conclusion to be drawn.

The model favours feedstocks with higher cellulose content for higher bio-oil and biofuel yields. This is also shown when comparing different soft- and hard-woods, the wood with a higher cellulose content gives a higher yield. This makes it so a one-on-one comparison of wood types is one dimensional and less accurate, as biochemical composition is not the only aspect affecting the bio-oil yield in real-life applications.

4.2. future recommendations

Model inconsistencies and suggestions for improvement:

- More complete process design, which reflects reality better with regards to parameters, blocks and overall process.
- More extensive kinetic network that has fewer simplifications and applies secondary reactions in the vapour phase.
- More extensive feedstock analysis in terms of biochemical composition, giving a more accurate representation of the feedstock. This is mainly for the lignin composition.

How to revisit the model and what to revisit:

- Techno economic analysis with eventual cost for fuel as outcome
- Comparison between different technologies for thermal conversion of lignocellulosic biomass. The model could be split in two, where the downstream processing can be applied to other technologies.

5. References

Alotaibi, M. A., Kozhevnikova, E. F., & Kozhevnikov, I. V. (2012). Deoxygenation of propionic acid on heteropoly acid and bifunctional metal-loaded heteropoly acid catalysts: Reaction pathways and turnover rates. *Applied Catalysis A: General*, *447–448*, 32–40. https://doi.org/10.1016/j.apcata.2012.08.042

Ansari, K. B., Arora, J. S., Chew, J. W., Dauenhauer, P. J., & Mushrif, S. H. (2019). Fast Pyrolysis of Cellulose, Hemicellulose, and Lignin: Effect of Operating Temperature on Bio-oil Yield and Composition and Insights into the Intrinsic Pyrolysis Chemistry. *Industrial and Engineering Chemistry Research*, *58*(35), 15838–15852. https://doi.org/10.1021/acs.iecr.9b00920

Aspen technology inc. (2013). *Aspen Physical Property Methods*. http://www.aspentech.com

Brandi, F., Bäumel, M., Shekova, I., Molinari, V., & Al-Naji, M. (2020). 5-Hydroxymethylfurfural Hydrodeoxygenation to 2,5-Dimethylfuran in Continuous-Flow System over Ni on Nitrogen-Doped Carbon. *Sustainable Chemistry*, *1*(2), 106–115. https://doi.org/10.3390/suschem1020009

Bridgwater, A. (2013). Fast pyrolysis of biomass for the production of liquids. In *Biomass Combustion Science, Technology and Engineering* (pp. 130–171). Elsevier Inc. https://doi.org/10.1533/9780857097439.2.130

Bridgwater, A. V. (2012). Review of fast pyrolysis of biomass and product upgrading. *Biomass and Bioenergy*, *38*, 68–94. https://doi.org/10.1016/j.biombioe.2011.01.048

Cuoci, A., Cuoci, A. O., Faravelli, T., Frassoldati, A., Granata, S., Migliavacca, G., Ranzi, E., & Sommariva, S. (n.d.). *A General Mathematical Model of Biomass Devolatilization Note 1. Lumped kinetic models of cellulose, hemicellulo... Comprehensive Kinet ic Modeling St udy of Bio-oil Format ion from Fast Pyrolysis of Biomass A General Mathematical Model of Biomass Devolatilization Note 1. Lumped kinetic models of cellulose, hemicellulose and lignin*.

Ding, Y., Ezekoye, O. A., Lu, S., Wang, C., & Zhou, R. (2017). Comparative pyrolysis behaviors and reaction mechanisms of hardwood and softwood. *Energy Conversion and Management*, *132*, 102–109. https://doi.org/10.1016/j.enconman.2016.11.016

European environment agency. (2024). *Use of renewable energy for transport in Europe*.

Frassoldati, A., Migliavacca, G., Crippa, T., Velata, F., Faravelli, T., & Ranzi, E. (n.d.). *Detailed Kinetic Modeling of Thermal Degradation of Biomasses*.

Gorensek, M. B., Shukre, R., & Chen, C. C. (2019). Development of a Thermophysical Properties Model for Flowsheet Simulation of Biomass Pyrolysis Processes. *ACS Sustainable Chemistry and Engineering*, *7*(9), 9017–9027. https://doi.org/10.1021/acssuschemeng.9b01278

Han, Y., Gholizadeh, M., Tran, C. C., Kaliaguine, S., Li, C. Z., Olarte, M., & Garcia-Perez, M. (2019a). Hydrotreatment of pyrolysis bio-oil: A review. In *Fuel Processing Technology* (Vol. 195). Elsevier B.V. https://doi.org/10.1016/j.fuproc.2019.106140

Han, Y., Gholizadeh, M., Tran, C. C., Kaliaguine, S., Li, C. Z., Olarte, M., & Garcia-Perez, M. (2019b). Hydrotreatment of pyrolysis bio-oil: A review. In *Fuel Processing Technology* (Vol. 195). Elsevier B.V. https://doi.org/10.1016/j.fuproc.2019.106140

Holum, M. L., & Jakobsen, T. G. (2024). Economic growth versus the environment: government spending, trust, and citizen support for environmental protection. *Environmental Sociology*. https://doi.org/10.1080/23251042.2024.2398503

Howe, D., Westover, T., Carpenter, D., Santosa, D., Emerson, R., Deutch, S., Starace, A., Kutnyakov, I., & Lukins, C. (2015). Field-to-fuel performance testing of lignocellulosic feedstocks: An integrated study of the fast pyrolysis-hydrotreating pathway. *Energy and Fuels*, *29*(5), 3188–3197. https://doi.org/10.1021/acs.energyfuels.5b00304

Jalid, F., Khan, T. S., Mir, F. Q., & Haider, M. A. (2017). Understanding trends in hydrodeoxygenation reactivity of metal and bimetallic alloy catalysts from ethanol reaction on stepped surface. *Journal of Catalysis*, *353*, 265–273. https://doi.org/10.1016/j.jcat.2017.07.018

Jongerius, A. L., Jastrzebski, R., Bruijnincx, P. C. A., & Weckhuysen, B. M. (2012). CoMo sulfide-catalyzed hydrodeoxygenation of lignin model compounds: An extended reaction network for the conversion of monomeric and dimeric substrates. *Journal of Catalysis*, *285*(1), 315–323. https://doi.org/10.1016/j.jcat.2011.10.006

Kargbo, H., Harris, J. S., & Phan, A. N. (2021). "Drop-in" fuel production from biomass: Critical review on techno-economic feasibility and sustainability. In *Renewable and Sustainable Energy Reviews* (Vol. 135). Elsevier Ltd. https://doi.org/10.1016/j.rser.2020.110168

Mishra, G., Kumar, J., & Bhaskar, T. (2015). Kinetic studies on the pyrolysis of pinewood. *Bioresource Technology*, *182*, 282–288. https://doi.org/10.1016/j.biortech.2015.01.087

Mu, W., Ben, H., Newalkar, G., Ragauskas, A., Qiu, D., & Deng, Y. (2014). Structure analysis of pine bark-, residue-, and stem-derived light oil and its hydrodeoxygenation products. *Industrial and Engineering Chemistry Research*, *53*(28), 11269–11275. https://doi.org/10.1021/ie500541p

Nyazika, T., Jimenez, M., Samyn, F., & Bourbigot, S. (2019). Pyrolysis modeling, sensitivity analysis, and optimization techniques for combustible materials: A review. *Journal of Fire Sciences*, *37*(4–6), 377–433. https://doi.org/10.1177/0734904119852740

Oasmaa, A., Solantausta, Y., Arpiainen, V., Kuoppala, E., & Sipilä, K. (2010). Fast pyrolysis bio-oils from wood and agricultural residues. *Energy and Fuels*, *24*(2), 1380–1388. https://doi.org/10.1021/ef901107f

Olarte, M. V., Padmaperuma, A. B., Ferrell, J. R., Christensen, E. D., Hallen, R. T., Lucke, R. B., Burton, S. D., Lemmon, T. L., Swita, M. S., Fioroni, G., Elliott, D. C., & Drennan, C. (2017). Characterization of upgraded fast pyrolysis oak oil distillate fractions from sulfided and non-sulfided catalytic hydrotreating. *Fuel*, *202*, 620–630. https://doi.org/10.1016/j.fuel.2017.03.051

Patel, M., & Kumar, A. (2016). Production of renewable diesel through the hydroprocessing of lignocellulosic biomass-derived bio-oil: A review. In *Renewable and Sustainable Energy Reviews* (Vol. 58, pp. 1293–1307). Elsevier Ltd. https://doi.org/10.1016/j.rser.2015.12.146

Peters, J. F., Banks, S. W., Bridgwater, A. V., & Dufour, J. (2017a). A kinetic reaction model for biomass pyrolysis processes in Aspen Plus. *Applied Energy*, *188*, 595–603. https://doi.org/10.1016/j.apenergy.2016.12.030

Peters, J. F., Banks, S. W., Bridgwater, A. V., & Dufour, J. (2017b). A kinetic reaction model for biomass pyrolysis processes in Aspen Plus. *Applied Energy*, *188*, 595–603. https://doi.org/10.1016/j.apenergy.2016.12.030

Ramzan, N., Ashraf, A., Naveed, S., & Malik, A. (2011). Simulation of hybrid biomass gasification using Aspen plus: A comparative performance analysis for food, municipal solid and poultry waste. *Biomass and Bioenergy*, *35*(9), 3962–3969. https://doi.org/10.1016/j.biombioe.2011.06.005

Rocha, A. S., Souza, L. A., Oliveira, R. R., Rocha, A. B., & Teixeira da Silva, V. (2017). Hydrodeoxygenation of acrylic acid using Mo2C/Al2O3. *Applied Catalysis A: General*, *531*, 69–78. https://doi.org/10.1016/j.apcata.2016.12.009

Schlaf, M., & Zhang, C. (2016). *Reaction Pathways and Mechanisms in Thermocatalytic Biomass Conversion II*. http://www.springer.com/series/11661

Shemfe, M. B., Gu, S., & Ranganathan, P. (2015). Techno-economic performance analysis of biofuel production and miniature electric power generation from biomass fast pyrolysis and bio-oil upgrading. *Fuel*, *143*, 361–372. https://doi.org/10.1016/j.fuel.2014.11.078

Suarez, M. Z., Moreno, F. P., Jurado, R. D. A., Valdes, R. M. A., & Comendador, V. F. G. (2024). An overview of the possibilities, current status, and limitations of battery technologies to electrify aviation. *Journal of Physics: Conference Series*, *2716*(1). https://doi.org/10.1088/1742-6596/2716/1/012012

Sullivan, M. M., & Bhan, A. (2016). Acetone Hydrodeoxygenation over Bifunctional Metallic-Acidic Molybdenum Carbide Catalysts. *ACS Catalysis*, *6*(2), 1145–1152. https://doi.org/10.1021/acscatal.5b02656

Wang, J., Bi, P., Zhang, Y., Xue, H., Jiang, P., Wu, X., Liu, J., Wang, T., & Li, Q. (2015). Preparation of jet fuel range hydrocarbons by catalytic transformation of bio-oil derived from fast pyrolysis of straw stalk. *Energy*, *86*, 488–499. https://doi.org/10.1016/j.energy.2015.04.053

Wooley, R. J., & Putsche, V. (n.d.-a). *Development of an ASPEN PLUS Physical Property Database for Biofuels Components*.

Wooley, R. J., & Putsche, V. (n.d.-b). *Development of an ASPEN PLUS Physical Property Database for Biofuels Components*.

World meteorological organization. (2023). *Greenhouse Gas concentrations hit record high. Again.*

Zhang, W., Zhang, Y., Zhao, L., & Wei, W. (2010). Catalytic activities of NiMo carbide supported on SiO2 for the hydrodeoxygenation of ethyl benzoate, acetone, and acetaldehyde. *Energy and Fuels*, *24*(3), 2052–2059. https://doi.org/10.1021/ef901222z

Zhao, C., He, J., Lemonidou, A. A., Li, X., & Lercher, J. A. (2011). Aqueous-phase hydrodeoxygenation of bio-derived phenols to cycloalkanes. *Journal of Catalysis*, *280*(1), 8–16. https://doi.org/10.1016/j.jcat.2011.02.001

Zhao, C., Jiang, E., & Chen, A. (2017). Volatile production from pyrolysis of cellulose, hemicellulose and lignin. *Journal of the Energy Institute*, *90*(6), 902–913. https://doi.org/10.1016/j.joei.2016.08.004

Alotaibi, M. A., Kozhevnikova, E. F., & Kozhevnikov, I. V. (2012). Deoxygenation of propionic acid on heteropoly acid and bifunctional metal-loaded heteropoly acid catalysts: Reaction pathways and turnover rates. *Applied Catalysis A: General*, *447–448*, 32–40. https://doi.org/10.1016/j.apcata.2012.08.042

Ansari, K. B., Arora, J. S., Chew, J. W., Dauenhauer, P. J., & Mushrif, S. H. (2019). Fast Pyrolysis of Cellulose, Hemicellulose, and Lignin: Effect of Operating Temperature on Bio-oil Yield and Composition and Insights into the Intrinsic Pyrolysis Chemistry. *Industrial and Engineering Chemistry Research*, *58*(35), 15838–15852. https://doi.org/10.1021/acs.iecr.9b00920

Aspen technology inc. (2013). *Aspen Physical Property Methods*. http://www.aspentech.com

Brandi, F., Bäumel, M., Shekova, I., Molinari, V., & Al-Naji, M. (2020). 5-Hydroxymethylfurfural Hydrodeoxygenation to 2,5-Dimethylfuran in Continuous-Flow System over Ni on Nitrogen-Doped Carbon. *Sustainable Chemistry*, *1*(2), 106–115. https://doi.org/10.3390/suschem1020009

Bridgwater, A. (2013). Fast pyrolysis of biomass for the production of liquids. In *Biomass Combustion Science, Technology and Engineering* (pp. 130–171). Elsevier Inc. https://doi.org/10.1533/9780857097439.2.130

Bridgwater, A. V. (2012). Review of fast pyrolysis of biomass and product upgrading. *Biomass and Bioenergy*, *38*, 68–94. https://doi.org/10.1016/j.biombioe.2011.01.048

Cuoci, A., Cuoci, A. O., Faravelli, T., Frassoldati, A., Granata, S., Migliavacca, G., Ranzi, E., & Sommariva, S. (n.d.). *A General Mathematical Model of Biomass Devolatilization Note 1. Lumped kinetic models of cellulose, hemicellulo... Comprehensive Kinet ic Modeling St udy of Bio-oil Format ion from Fast Pyrolysis of Biomass A General Mathematical Model of Biomass Devolatilization Note 1. Lumped kinetic models of cellulose, hemicellulose and lignin*.

Ding, Y., Ezekoye, O. A., Lu, S., Wang, C., & Zhou, R. (2017). Comparative pyrolysis behaviors and reaction mechanisms of hardwood and softwood. *Energy Conversion and Management*, *132*, 102–109. https://doi.org/10.1016/j.enconman.2016.11.016

European environment agency. (2024). *Use of renewable energy for transport in Europe*.

Frassoldati, A., Migliavacca, G., Crippa, T., Velata, F., Faravelli, T., & Ranzi, E. (n.d.). *Detailed Kinetic Modeling of Thermal Degradation of Biomasses*.

Gorensek, M. B., Shukre, R., & Chen, C. C. (2019). Development of a Thermophysical Properties Model for Flowsheet Simulation of Biomass Pyrolysis Processes. *ACS Sustainable Chemistry and Engineering*, *7*(9), 9017–9027. https://doi.org/10.1021/acssuschemeng.9b01278

Han, Y., Gholizadeh, M., Tran, C. C., Kaliaguine, S., Li, C. Z., Olarte, M., & Garcia-Perez, M. (2019a). Hydrotreatment of pyrolysis bio-oil: A review. In *Fuel Processing Technology* (Vol. 195). Elsevier B.V. https://doi.org/10.1016/j.fuproc.2019.106140

Han, Y., Gholizadeh, M., Tran, C. C., Kaliaguine, S., Li, C. Z., Olarte, M., & Garcia-Perez, M. (2019b). Hydrotreatment of pyrolysis bio-oil: A review. In *Fuel Processing Technology* (Vol. 195). Elsevier B.V. https://doi.org/10.1016/j.fuproc.2019.106140

Holum, M. L., & Jakobsen, T. G. (2024). Economic growth versus the environment: government spending, trust, and citizen support for environmental protection. *Environmental Sociology*. https://doi.org/10.1080/23251042.2024.2398503

Howe, D., Westover, T., Carpenter, D., Santosa, D., Emerson, R., Deutch, S., Starace, A., Kutnyakov, I., & Lukins, C. (2015). Field-to-fuel performance testing of lignocellulosic feedstocks: An integrated study of the fast pyrolysis-hydrotreating pathway. *Energy and Fuels*, *29*(5), 3188–3197. https://doi.org/10.1021/acs.energyfuels.5b00304

Jalid, F., Khan, T. S., Mir, F. Q., & Haider, M. A. (2017). Understanding trends in hydrodeoxygenation reactivity of metal and bimetallic alloy catalysts from ethanol reaction on stepped surface. *Journal of Catalysis*, *353*, 265–273. https://doi.org/10.1016/j.jcat.2017.07.018

Jongerius, A. L., Jastrzebski, R., Bruijnincx, P. C. A., & Weckhuysen, B. M. (2012). CoMo sulfide-catalyzed hydrodeoxygenation of lignin model compounds: An extended reaction network for the conversion of monomeric and dimeric substrates. *Journal of Catalysis*, *285*(1), 315–323. https://doi.org/10.1016/j.jcat.2011.10.006

Kargbo, H., Harris, J. S., & Phan, A. N. (2021). "Drop-in" fuel production from biomass: Critical review on techno-economic feasibility and sustainability. In *Renewable and Sustainable Energy Reviews* (Vol. 135). Elsevier Ltd. https://doi.org/10.1016/j.rser.2020.110168

Mishra, G., Kumar, J., & Bhaskar, T. (2015). Kinetic studies on the pyrolysis of pinewood. *Bioresource Technology*, *182*, 282–288. https://doi.org/10.1016/j.biortech.2015.01.087

Mu, W., Ben, H., Newalkar, G., Ragauskas, A., Qiu, D., & Deng, Y. (2014). Structure analysis of pine bark-, residue-, and stem-derived light oil and its hydrodeoxygenation products. *Industrial and Engineering Chemistry Research*, *53*(28), 11269–11275. https://doi.org/10.1021/ie500541p

Nyazika, T., Jimenez, M., Samyn, F., & Bourbigot, S. (2019). Pyrolysis modeling, sensitivity analysis, and optimization techniques for combustible materials: A review. *Journal of Fire Sciences*, *37*(4–6), 377–433. https://doi.org/10.1177/0734904119852740

Oasmaa, A., Solantausta, Y., Arpiainen, V., Kuoppala, E., & Sipilä, K. (2010). Fast pyrolysis bio-oils from wood and agricultural residues. *Energy and Fuels*, *24*(2), 1380–1388. https://doi.org/10.1021/ef901107f

Olarte, M. V., Padmaperuma, A. B., Ferrell, J. R., Christensen, E. D., Hallen, R. T., Lucke, R. B., Burton, S. D., Lemmon, T. L., Swita, M. S., Fioroni, G., Elliott, D. C., & Drennan, C. (2017). Characterization of upgraded fast pyrolysis oak oil distillate fractions from sulfided and non-sulfided catalytic hydrotreating. *Fuel*, *202*, 620–630. https://doi.org/10.1016/j.fuel.2017.03.051

Patel, M., & Kumar, A. (2016). Production of renewable diesel through the hydroprocessing of lignocellulosic biomass-derived bio-oil: A review. In *Renewable and Sustainable Energy Reviews* (Vol. 58, pp. 1293–1307). Elsevier Ltd. https://doi.org/10.1016/j.rser.2015.12.146

Peters, J. F., Banks, S. W., Bridgwater, A. V., & Dufour, J. (2017a). A kinetic reaction model for biomass pyrolysis processes in Aspen Plus. *Applied Energy*, *188*, 595–603. https://doi.org/10.1016/j.apenergy.2016.12.030

Peters, J. F., Banks, S. W., Bridgwater, A. V., & Dufour, J. (2017b). A kinetic reaction model for biomass pyrolysis processes in Aspen Plus. *Applied Energy*, *188*, 595–603. https://doi.org/10.1016/j.apenergy.2016.12.030

Ramzan, N., Ashraf, A., Naveed, S., & Malik, A. (2011). Simulation of hybrid biomass gasification using Aspen plus: A comparative performance analysis for food, municipal solid and poultry waste. *Biomass and Bioenergy*, *35*(9), 3962–3969. https://doi.org/10.1016/j.biombioe.2011.06.005

Rocha, A. S., Souza, L. A., Oliveira, R. R., Rocha, A. B., & Teixeira da Silva, V. (2017). Hydrodeoxygenation of acrylic acid using Mo2C/Al2O3. *Applied Catalysis A: General*, *531*, 69–78. https://doi.org/10.1016/j.apcata.2016.12.009

Schlaf, M., & Zhang, C. (2016). *Reaction Pathways and Mechanisms in Thermocatalytic Biomass Conversion II*. http://www.springer.com/series/11661

Shemfe, M. B., Gu, S., & Ranganathan, P. (2015). Techno-economic performance analysis of biofuel production and miniature electric power generation from biomass fast pyrolysis and bio-oil upgrading. *Fuel*, *143*, 361–372. https://doi.org/10.1016/j.fuel.2014.11.078

Suarez, M. Z., Moreno, F. P., Jurado, R. D. A., Valdes, R. M. A., & Comendador, V. F. G. (2024). An overview of the possibilities, current status, and limitations of battery technologies to electrify aviation. *Journal of Physics: Conference Series*, *2716*(1). https://doi.org/10.1088/1742-6596/2716/1/012012

Sullivan, M. M., & Bhan, A. (2016). Acetone Hydrodeoxygenation over Bifunctional Metallic-Acidic Molybdenum Carbide Catalysts. *ACS Catalysis*, *6*(2), 1145–1152. https://doi.org/10.1021/acscatal.5b02656

Wang, J., Bi, P., Zhang, Y., Xue, H., Jiang, P., Wu, X., Liu, J., Wang, T., & Li, Q. (2015). Preparation of jet fuel range hydrocarbons by catalytic transformation of bio-oil derived from fast pyrolysis of straw stalk. *Energy*, *86*, 488–499. https://doi.org/10.1016/j.energy.2015.04.053

Wooley, R. J., & Putsche, V. (n.d.-a). *Development of an ASPEN PLUS Physical Property Database for Biofuels Components*.

Wooley, R. J., & Putsche, V. (n.d.-b). *Development of an ASPEN PLUS Physical Property Database for Biofuels Components*.

World meteorological organization. (2023). *Greenhouse Gas concentrations hit record high. Again.*

Zhang, W., Zhang, Y., Zhao, L., & Wei, W. (2010). Catalytic activities of NiMo carbide supported on SiO2 for the hydrodeoxygenation of ethyl benzoate, acetone, and acetaldehyde. *Energy and Fuels*, *24*(3), 2052–2059. https://doi.org/10.1021/ef901222z

Zhao, C., He, J., Lemonidou, A. A., Li, X., & Lercher, J. A. (2011). Aqueous-phase hydrodeoxygenation of bio-derived phenols to cycloalkanes. *Journal of Catalysis*, *280*(1), 8–16. https://doi.org/10.1016/j.jcat.2011.02.001

Zhao, C., Jiang, E., & Chen, A. (2017). Volatile production from pyrolysis of cellulose, hemicellulose and lignin. *Journal of the Energy Institute*, *90*(6), 902–913. https://doi.org/10.1016/j.joei.2016.08.004

6. Appendix

6.1. HDO reactions

FORMULA	COMPOUND	KG/H	C	H	O
C2H4O2	GLYCO-01	216,215	2	4	2
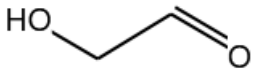	C2H4O2 + 3H2 → C2H6 + 2H2O (Nyazika et al., 2019)				
C2H2O2	GLYOX-01	54,989	2	2	2
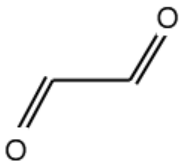	C2H2O2 +4H2 → C2H6 + 2H2O (Schlaf & Zhang, 2016)				
C2H4O	ACETA-01	33,867	2	4	1
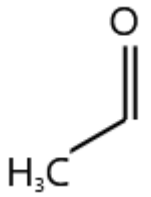	C2H4O + 2H2 → C2H6 + H2O (Sullivan & Bhan, 2016)				
C3H6O	ACETO-01	84,244	3	6	1
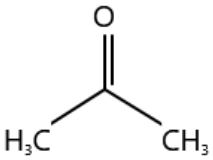	C3H6O + 2H2 → C3H8 + H2O (Zhang et al., 2010)				
C6H6O3	5-HYD-01	119,488	6	6	3
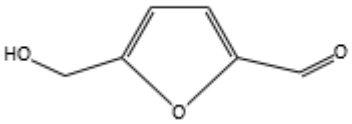	C6H6O3 + 3H2 → C6H8O + 2H2O (Brandi et al., 2020)				
C3H6O2	PROPI-01	0,799	3	6	2
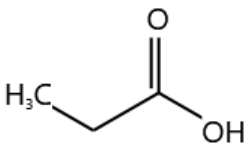	C3H6O2 + H2 → C3H6O + H2O (Alotaibi et al., 2012)				
C6H6O	PHENO-01	8,971	6	6	1
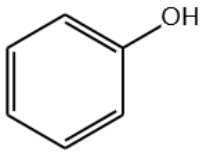	C6H6O + 4H2 → C6H12 + H2O (Zhao et al., 2011)				

Formula	Compound	Kg/h	C	H	O
C2H6O	ETHAN-01	36,143	2	6	1
	2C2H6O → CH4 + CO + C2H6 + H2O (Jalid et al., 2017)				
CH2O	FORMA-01	270,89	1	2	1
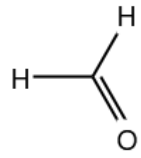					
C6H10O5	LEVOG-01	863,181	6	10	5
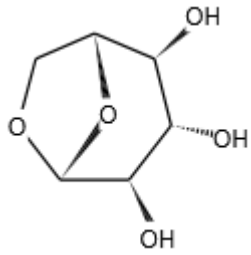	C6H10O5 + 5H2 → C6H12O + 4H2O (Mu et al., 2014)				
C11H12O4	SINAPYL	71,436	11	12	4
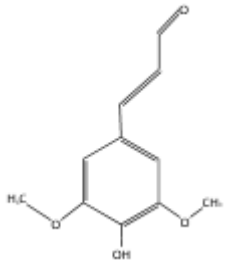	C11H12O4 + 7H2 → C9H10 + 2CH4 + 4H2O (Jongerius et al., 2012)				
C9H10O2	P-COUMAR	17,968	9	10	2
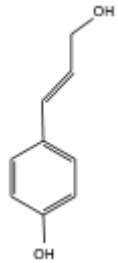	C9H10O2 + 2H2 → C9H10 + 2H2O (Jongerius et al., 2012)				

Formula	Compound	Kg/h	C	H	O
C5H10O5	XYLOSE	0,072	5	10	5
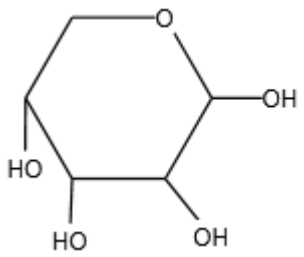	C5H10O5 + 4H2 → C5H10O + 4H2O (Schlaf & Zhang, 2016)				
CH4O	METHANOL	63,799	1	4	1
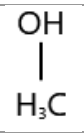					
C2H4	ETHENE	0,825	2	4	0
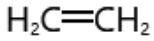					
C3H4O2	ACRYL-01	0,247	3	4	2
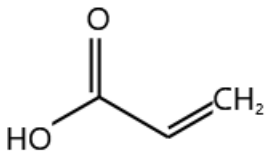	C3H4O2 + 4H2 → C3H8 + 2H2O (Rocha et al., 2017)				

6.2. Model summary

Heater

Name	CONDENSE	HEAT1
Property method	**PR-BM**	**NRTL-RK**
Henry's component list ID		
Electrolyte chemistry ID		
Use true species approach for electrolytes	**YES**	**YES**
Free-water phase properties method	**STEAM-TA**	**STEAM-TA**
Water solubility method	**3**	**3**
Specified pressure [bar]	**10**	**3**
Specified temperature [C]	**20**	**200**
Specified vapor fraction		
Specified heat duty [cal/sec]		
EO Model components		
Calculated pressure [atm]	9,86923267	2,9607698
Calculated temperature [K]	293,15	473,15
Calculated vapor fraction	0,852511261	1
Calculated heat duty [cal/sec]	-406155,099	-26563,6926
Temperature change [K]		
Degrees of superheating [K]		
Degrees of subcooling [K]		
Pressure-drop correlation parameter		
Net duty [cal/sec]	-406155,099	-26563,6926
First liquid / total liquid	0,386146351	
Total feed stream CO2e flow [kg/hr]	474,757602	0
Total product stream CO2e flow [kg/hr]	474,757602	0
Net stream CO2e production [kg/hr]	0	0
Utility CO2e production [kg/hr]	0	0
Total CO2e production [kg/hr]	0	0
Utility usage		
Utility cost		
Utility ID		

FLASH2		
Name	DRY-FLSH	FLASH
Property method	**PR-BM**	**PR-BM**
Henry's component list ID		
Electrolyte chemistry ID		
Use true species approach for electrolytes	**YES**	**YES**
Free-water phase properties method	**STEAM-TA**	**STEAM-TA**
Water solubility method	**3**	**3**
Temperature [K]		**20**
Pressure [atm]	**1,000275669**	**10**
Specified vapor fraction		
Specified heat duty [cal/sec]	**0**	
EO Model components		
Outlet temperature [K]	313,350632	293,15
Outlet pressure [atm]	1,00027567	9,86923267
Vapor fraction	1	0,854262976
Heat duty [cal/sec]	0	1415,01195
Net duty [cal/sec]	0	1415,01195
First liquid / total liquid		0,33959709
Total feed stream CO2e flow [kg/hr]	0	474,757602
Total product stream CO2e flow [kg/hr]	0	474,757563
Net stream CO2e production [kg/hr]	0	-3,84153E-05
Utility CO2e production [kg/hr]	0	0
Total CO2e production [kg/hr]	0	-3,84153E-05
Utility usage		
Utility cost		
Utility ID		

SEP			
Name	CYCLONE	OFFGAS2	POLAR
Property method	**PR-BM**	**PR-BM**	**PR-BM**
Henry's component list ID			
Electrolyte chemistry ID			
Use true species approach for electrolytes	**YES**	**YES**	**YES**
Free-water phase properties method	**STEAM-TA**	**STEAM-TA**	**STEAM-TA**
Water solubility method	**3**	**3**	**3**
Inlet flash pressure [atm]	**0**	**0**	**0**
First outlet flash temperature			
First outlet flash pressure			
First outlet flash temperature change			
First outlet flash vapor fraction			
First outlet flash temperature estimate			
First outlet flash pressure estimate			
Second outlet flash temperature			
Second outlet flash pressure			
Second outlet flash temperature change			
Second outlet flash vapor fraction			
Second outlet flash temperature estimate			
Second outlet flash pressure estimate			
EO Model components			
Heat duty [cal/sec]	-5,86892E-05	-2,02803735	-63,981859
Total feed stream CO2e flow [kg/hr]	474,757602	287,585014	0
Total product stream CO2e flow [kg/hr]	474,757602	287,585014	0
Net stream CO2e production [kg/hr]	0	0	0
Utility CO2e production [kg/hr]	0	0	0
Total CO2e production [kg/hr]	0	0	0
Utility usage			
Utility cost			
Utility ID			

RADFRAC		
Name	DISTIL1	DISTIL2
Property method	**NRTL-RK**	**NRTL-RK**
Henry's component list ID		
Electrolyte chemistry ID		
Use true species approach for electrolytes	**YES**	**YES**
Free-water phase properties method	**STEAM-TA**	**STEAM-TA**
Water solubility method	**3**	**3**
Number of stages	**7**	**3**
Condenser	**PARTIAL-V-L**	**PARTIAL-V-L**
Reboiler	**KETTLE**	**KETTLE**
Number of phases	**2**	**2**
Free-water	**NO**	**NO**
Top stage pressure [bar]	**2,9**	**1,5**
Specified reflux ratio	**1**	**1**
Specified bottoms rate [kg/hr]		
Specified boilup rate [kg/hr]		
Specified distillate rate [kg/hr]		
EO Model components		
Calculated molar reflux ratio	0,950640475	1
Calculated bottoms rate [kmol/hr]	6,22371223	2,65632313
Calculated boilup rate [kmol/hr]	18047,9888	5,90774879
Calculated distillate rate [kmol/hr]	9,66377753	3,5673891
Condenser / top stage temperature [K]	150,483959	389,895502
Condenser / top stage pressure [atm]	2,86207747	1,4803849
Condenser / top stage heat duty [cal/sec]	-72173656,1	-15477,0749
Condenser / top stage subcooled duty		
Condenser / top stage reflux rate [kmol/hr]	9,18677807	3,5673891
Condenser / top stage free water reflux ratio		
Reboiler pressure [atm]	2,86207747	1,4803849
Reboiler temperature [K]	419,369212	396,771564
Reboiler heat duty [cal/sec]	37770493,4	12901,4091
Total feed stream CO2e flow [kg/hr]	0	0
Total product stream CO2e flow [kg/hr]	0	0
Net stream CO2e production [kg/hr]	0	0
Utility CO2e production [kg/hr]	0	0
Total CO2e production [kg/hr]	0	0
Condenser utility usage		
Condenser utility cost		
Condenser utility ID		
Reboiler utility usage		
Reboiler utility cost		
Reboiler utility ID		
Basis for specified distillate to feed ratio	**MASS**	**MASS**

Specified distillate to feed ratio	**0,3**	**0,565**
Basis for specified bottoms to feed ratio	**MASS**	**MASS**
Specified bottoms to feed ratio		
Basis for specified boilup ratio	**MASS**	**MASS**
Specified boilup ratio		
Calculated molar boilup ratio	2899,8752	2,22403243
Calculated mass boilup ratio	2809,92967	2,17688192

RSTOIC

Name	DRYER	HDO
Property method	**PR-BM**	**PR-BM**
Henry's component list ID		
Electrolyte chemistry ID		
Use true species approach for electrolytes	**YES**	**YES**
Free-water phase properties method	**STEAM-TA**	**STEAM-TA**
Water solubility method	**3**	**3**
Specified pressure [atm]	**1,00028**	**1**
Specified temperature [K]		**400**
Specified vapor fraction		
Specified heat duty [cal/sec]	**0**	
EO Model components		
Outlet temperature [K]	313,350634	673,15
Outlet pressure [atm]	1,00028	1
Calculated heat duty [cal/sec]	0	26499920,8
Net heat duty [cal/sec]	0	26499920,8
Calculated vapor fraction	1	1
First liquid / total liquid		
Total feed stream CO2e flow [kg/hr]	0	1,08361157
Total product stream CO2e flow [kg/hr]	0	287,585014
Net stream CO2e production [kg/hr]	0	286,501403
Utility CO2e production [kg/hr]	0	0
Total CO2e production [kg/hr]	0	286,501403
Utility usage		
Utility cost		
Utility ID		

RYIELD	
Name	DECOMP
Property method	**PR-BM**
Henry's component list ID	
Electrolyte chemistry ID	
Use true species approach for electrolytes	**YES**
Free-water phase properties method	**STEAM-TA**
Water solubility method	**3**
Specified pressure [atm]	**1,000275669**
Specified temperature [K]	**294,2611111**
Specified temperature change [K]	
Specified vapor fraction	
Specified heat duty [cal/sec]	**0**
EO Model components	
Outlet temperature [K]	294,261111
Outlet pressure [atm]	1,00027567
Calculated heat duty [cal/sec]	50744,0484
Net heat duty [cal/sec]	50744,0484
Calculated vapor fraction	1
Calculated temperature change	
Total feed stream CO2e flow [kg/hr]	0
Total product stream CO2e flow [kg/hr]	0
Net stream CO2e production [kg/hr]	0
Utility CO2e production [kg/hr]	0
Total CO2e production [kg/hr]	0
Utility usage	
Utility cost	
Utility ID	

RCSTR	
Name	KINETICS
Property method	**PR-BM**
Henry's component list ID	
Electrolyte chemistry ID	
Use true species approach for electrolytes	**YES**
Free-water phase properties method	**STEAM-TA**
Water solubility method	**3**
Specified pressure [atm]	**20**
Specified temperature [C]	**500**
Specified heat duty [cal/sec]	
Reactor volume [l]	**1000**
Reactor residence time [sec]	**2**
Phase volume [l]	
Phase volume frac	
Phase residence time [hr]	
EO Model components	
Outlet temperature [K]	773,15
Calculated heat duty [cal/sec]	-26046091,1
Net heat duty [cal/sec]	-26046091,1
Reactor volume [l]	409,465764
Vapor phase volume [l]	409,208986
Liquid phase volume [l]	0
Liquid 1 phase volume	
Salt phase volume	
Condensed phase volume [l]	0,256778417
Reactor residence time [hr]	0,000555556
Vapor phase residence time [hr]	0,000555556
Condensed phase residence time [hr]	0,000555556
Total feed stream CO2e flow [kg/hr]	0
Total product stream CO2e flow [kg/hr]	474,757602
Net stream CO2e production [kg/hr]	474,757602
Utility CO2e production [kg/hr]	0
Total CO2e production [kg/hr]	474,757602
Utility usage	
Utility cost	
Utility ID	

6.3. User defined components

Estimated property model parameters for solid components added outside of database (Wooley & Putsche, n.d.-b).

COMPONENT	CHEMICAL STRUCTURE	MOLECULAR WEIGHT	SOLID ENTHALPY OF FORMATION (KJ/KMOL)	SOLID MOLAR HEAT CAPACITY (KJ/KMOL-K)	SOLID MOLAR VOLUME (ML/MOL)
Hemicellulose	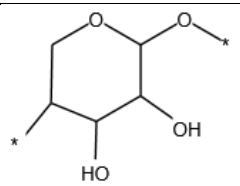	132,11	--759200	162,72	86,92
Cellulose	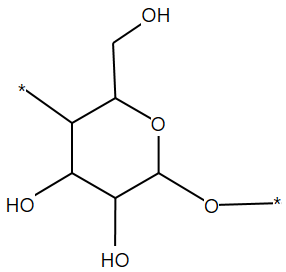	162,1424	-1019000	199,70	106,67
Cellulose (A)	See cellulose				
Hemicellulose (1)	See hemicellulose				
Hemicellulose (2)	See hemicellulose				
Lignin-C	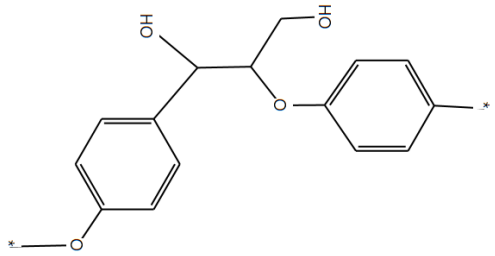	258,27	-759390	322,59	169,92
Lignin-CC	See Lignin-C				

COMPONENT	CHEMICAL STRUCTURE	MOLECULAR WEIGHT	SOLID ENTHALPY OF FORMATION (KJ/KMOL)	SOLID MOLAR HEAT CAPACITY (KJ/KMOL-K)	SOLID MOLAR VOLUME (ML/MOL)
Lignin-H	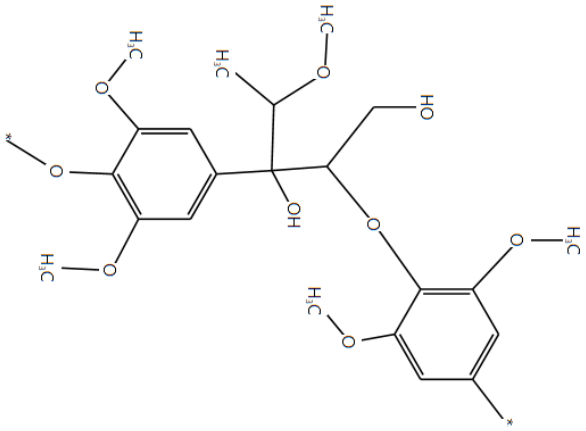	436,45	-1722700	545,15	287,14
Lignin-OH	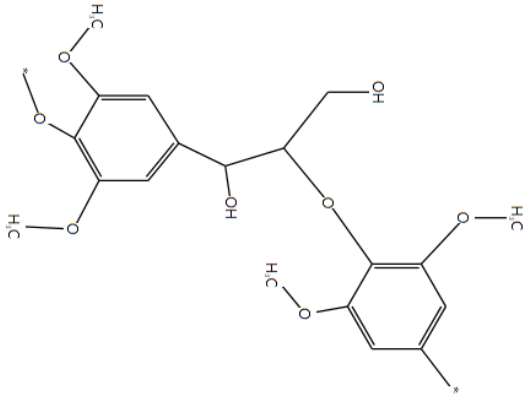	378,37	-1429200	472,60	248,94

COMPONENT	CHEMICAL STRUCTURE	MOLECULAR WEIGHT	SOLID ENTHALPY OF FORMATION (KJ/KMOL)	SOLID MOLAR HEAT CAPACITY (KJ/KMOL-K)	SOLID MOLAR VOLUME (ML/MOL)
Lignin-O	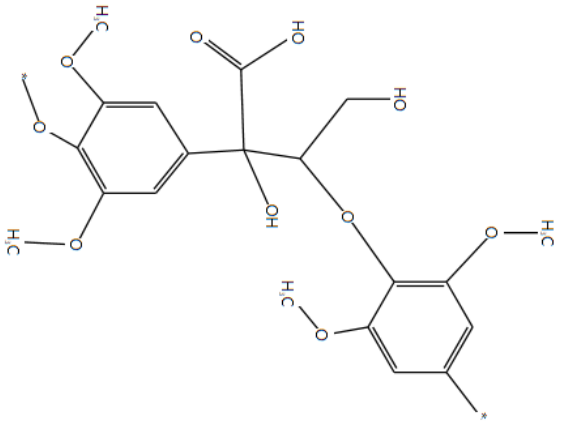	422,38	-1847500	527,57	277,89
Lig	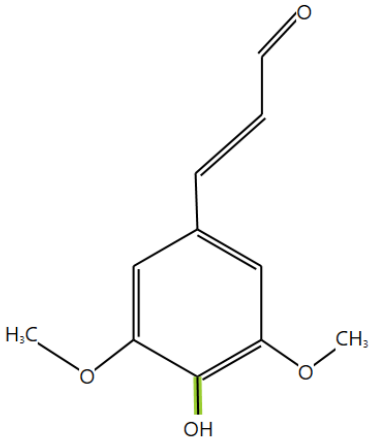	208,21	-729310	260,06	136,98

Estimated property model parameters for conventional components added outside of database.

P-coumaryl alcohol		
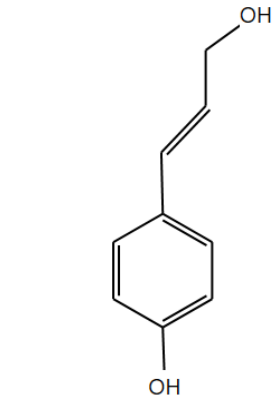	Molecular weight (g/mol)	150,17
	Ideal gas standard heat of formation (kJ/mol)	-193,5
	Critical temperature (K)	791,4
	Critical pressure (bar)	56,9
	Acentric factor	1,198
	Vapor pressure	See (Gorensek et al., 2019) for polynomial range
	Ideal gas molar heat capacity	See (Gorensek et al., 2019) for polynomial range
Sinapyl aldehyde		
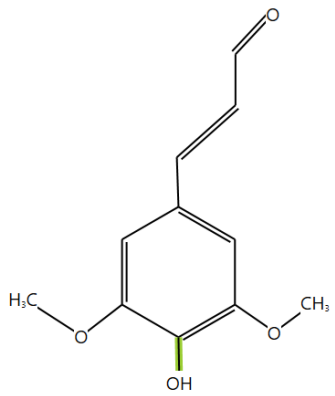	Molecular weight (g/mol)	208,21
	Ideal gas standard heat of formation (kJ/mol)	-483,8
	Critical temperature (K)	837,9
	Critical pressure (bar)	29,25
	Acentric factor	0,981
	Vapor pressure	See (Gorensek et al., 2019) for polynomial range
	Ideal gas molar heat capacity	See (Gorensek et al., 2019) for polynomial range

6.4. Biochemical composition for different wood types

Biochemical composition of two hard- and two soft-woods.

	SPECIES	SOURCE	CELLULOSE	HEMICELLULOSE	LIGNIN
Hard	Eucalyptus	(Oasmaa et al., 2010)	46,25	18,5	25,9
Hard	Beech	(Peters et al., 2017b)	42,78	23,04	21,16
Soft	Pine	(Oasmaa et al., 2010)	40,24	14,34	14,34
Soft	Chinese Fir	(Ding et al., 2017)	45,23	11,01	28,86